UNIVERSIDADE DE SÃO PAULO

IGOR DE PAULA MOURA

Integration of bi-reforming of methane with ammonia and urea processes

São Paulo

2021

IGOR DE PAULA MOURA

Integration of bi-reforming of methane with ammonia and urea processes

Corrected Version

Master dissertation presented to the Graduate Program in Chemical Engineering at the Escola Politécnica da Universidade de São Paulo to obtain the degree of Master of Science.

Concentration Area: Chemical Engineering

Advisor: Prof. Dr. Rita Maria de Brito Alves
Co-advisor: Dr. Alessandra Carvalho Reis

São Paulo
2021

Autorizo a reprodução e divulgação total ou parcial deste trabalho, por qualquer meio convencional ou eletrônico, para fins de estudo e pesquisa, desde que citada a fonte.

Este exemplar foi revisado e corrigido em relação à versão original, sob responsabilidade única do autor e com a anuência de seu orientador.

São Paulo, 10 de março de 2021.

Assinatura do autor: 

Assinatura do orientador: 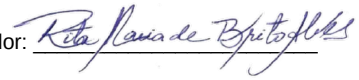

Catalogação-na-publicação

Moura, Igor
Integration of bi-reforming of methane with ammonia and urea processes / I. Moura -- versão corr. -- São Paulo, 2021.
102 p.

Dissertação (Mestrado) - Escola Politécnica da Universidade de São Paulo. Departamento de Engenharia Química.

1.Birreforma de metano 2.Abatimento de CO2 3.<Amônia>[Síntese] I.Universidade de São Paulo. Escola Politécnica. Departamento de Engenharia Química II.t.

Name: Moura, Igor de Paula

Title: Integration of bi-reforming of methane with ammonia and urea processes.

Master dissertation presented to the Graduate Program in Chemical Engineering at the Escola Politécnica da Universidade de São Paulo to obtain the degree of Master of Science.

Approved on: 13/Jan/2021

Examining Commission

Prof. Dr.: Rita Maria de Brito Alves
Institution: Escola Politécnica da Universidade de São Paulo
Evaluation: Approved

Prof. Dr.: Paulo Luiz de Andrade Coutinho
Institution: External
Evaluation: Approved

Prof. Dr.: Ana Paula Santana Musse
Institution: External
Evaluation: Approved

ACKNOWLEDGMENTS

I would like to thank my advisor, Prof. Rita Maria de Brito Alves, my co-advisor, Dr. Alessandra de Carvalho Reis, and Dr. Antonio Esio Bresciani for their support, their helpful knowledge, and the opportunity they have given me to develop this work at the Universidade de São Paulo.

Gratitude, as well, to all my colleagues from the LSCP, the laboratory where this dissertation was developed. Whether they spent some time helping me with an apparently impossible problem encountered, or just took their time to have a coffee with me to settle my thoughts down, they deserve my humble thanks. Every day is a struggle, and having the right people nearby makes things more bearable for everyone.

I also would like to thank my mother for her immense support. This work was only possible thanks to her constant encouragement throughout this program.

More than just a title of Master of Science, this journey gave me a new vision of life. There have been ups and downs, and true friends support you even when you are at your worst. Special thanks to João Vitor Lopes Monteiro and Maria Clara Mendes da Silva for supporting me even when everything seemed impossible, including getting out of bed.

Finally, I gratefully acknowledge the support of the RCGI – Research Centre for Gas Innovation, hosted by the University of São Paulo (USP) and sponsored by FAPESP – São Paulo Research Foundation (2014/50279-4) and Shell Brasil, and the strategic importance of the support given by ANP (Brazil's National Oil, Natural Gas and Biofuels Agency) through the R&D levy regulation.

“There is a single light of science,
and to brighten it anywhere
is to brighten it everywhere.”
Isaac Asimov

ABSTRACT

MOURA, I. P.; Integration of bi-reforming of methane with ammonia and urea processes. Universidade de São Paulo, 2021.

Recently in Brazil, thermal power plants have had their use increased as a source of energy generation, despite these being associated with increased greenhouse gases emissions, especially carbon dioxide (CO_2). In the context of the Paris Agreement of 2015, carbon capture, utilization, and storage techniques must be increasingly employed to mitigate environmental issues. In this scenario, the utilization of CO_2 coming from a power plant flue gas as feedstock for other chemical synthesis arises as a good alternative to achieve near-zero CO_2 emissions. For this, the integration of a power plant with an industrial process that requires external CO_2 streams is a viable option. This way, an alternative configuration for ammonia and urea production was proposed in order to take advantage of this synergy. The proposed configuration includes a bi-reforming process, an ammonia synthesis loop, a urea reactor, and auxiliary units to achieve CO_2 abatement and high-value product generation. Computer simulations with Aspen Plus were carried out to find the operational parameters for the configuration. Technical, economic, and environmental performances of both the proposed configuration and the conventional configuration based on steam reforming were also compared. Results show that the innovative configuration has better economic parameters, although both configurations are not profitable depending on natural gas prices. However, the innovative configuration has the potential to abate 30.64 tonnes of CO_2 per hour (equivalent to 268410 tonnes per year).

Keywords: CO_2 conversion, CO_2 abatement, bi-reforming of methane, ammonia synthesis, process integration.

RESUMO

MOURA, I. P.; Integration of bi-reforming of methane with ammonia and urea processes. Universidade de São Paulo, 2021.

Recentemente, no Brasil, o uso de termelétricas como fontes de geração de energia vem crescendo, apesar de essas estarem associadas ao aumento das emissões de gases do efeito estufa, principalmente o dióxido de carbono (CO_2). De acordo com o Acordo de Paris de 2015, captura, utilização e estocagem de carbono devem ter seus usos ampliados para mitigar os problemas ambientais. Nesse contexto, uma boa alternativa para atingir emissões quase-nulas de CO_2 é o uso direto, como por exemplo, a corrente de saída de uma termelétrica, como matéria-prima para a produção de produtos químicos. Para isso, uma opção viável é a integração entre uma termelétrica e processos industriais que necessitam de correntes de CO_2. Para tirar proveito dessa sinergia, foi proposta uma configuração alternativa para a produção de amônia e ureia. Essa configuração inclui um reator de birreforma de metano, um *loop* de síntese de amônia, um reator de ureia e unidades auxiliares, de modo a promover o abatimento de CO_2 e geração de produtos de alto valor agregado. Simulações computacionais com Aspen Plus foram utilizadas para estabelecer os parâmetros operacionais da configuração proposta. Parâmetros técnicos, econômicos e ambientais tanto da configuração proposta quanto da configuração convencional, baseada na reforma a vapor de metano, foram comparados. Resultados mostram que a rota inovativa apresenta melhores indicadores econômicos, apesar de ambas as configurações não serem lucrativas, dependendo do preço de compra do gás natural. Além disso, a configuração inovativa possui potencial para abater 30,64 toneladas de CO_2 por hora (equivalente a 268410 toneladas por ano).

Palavras-chave: conversão de CO_2, abatimento de CO_2, birreforma de metano, síntese de amônia, integração de processos.

LIST OF FIGURES

LIST OF TABLES

LIST OF ABBREVIATIONS AND ACRONYMS

ASR	Ammonia Synthesis Reaction
BR	Bi-reformer
BRM	Bi-reforming of Methane
CAPEX	Capital Expenditure
CCUS	Carbon Capture, Utilization, and Storage
CDU	Carbon Dioxide Utilization
CEPCI	Chemical Engineering Plant Cost Index
CW	Cooling Water
DRM	Dry Reforming of Methane
ECI	Electric Carbon Intensity
EEI	Electric Energy Intensity
EIA	Energy Information Administration
ELEC	Electricity
EPA	Environmental Protection Agency
FAPESP	Fundação de Amparo à Pesquisa do Estado de São Paulo
FH	Fired Heater
GCI	Global Carbon Intensity
GHG	Greenhouse Gases
GHSV	Gas Hourly Space Velocity
HPS	High-Pressure Steam
HPSg	High-Pressure Steam Generation
HTS	High-Temperature Shift
IHS	Information Handling Services
LPS	Low-Pressure Steam
LPSg	Low-Pressure Steam Generation
LSCP	Laboratório de Simulação e Controle de Processos
LTS	Low-Temperature Shift
MACRS	Modified Accelerated Cost Recovery System
MEA	Monoethanolamine
MET	Methanation
MM$	Millions of US dollars

MPS	Medium-Pressure Steam
MPSg	Medium-Pressure Steam Generation
MRM	Matrix Reduction Method
MTPD	Metric Tonnes Per Day
NG	Natural Gas
NHV	Net Heating Value
NPV	Net Present Value
OPEX	Operational Expenditure
PFD	Process Flow Diagram
POM	Partial Oxidation of Methane
PSA	Pressure Swing Adsorption
RCGI	Research Centre for Gas Innovation
RM	Raw Material
RWGS	Reverse Water-Gas Shift
SDR	Secondary Reformer
SR	Steam Reformer
SRM	Steam Reforming of Methane
TCI	Thermal Carbon Intensity
TEI	Thermal Energy Intensity
TRL	Technology Readiness Level
TRM	Tri-Reforming of Methane
WGS	Water-Gas Shift

SUMMARY

1. INTRODUCTION

To reduce greenhouse gas (GHG) emissions (especially CO_2, which consists of 72% of the GHG emissions (OLIVIER; SCHURE; PETERS, 2018)), carbon capture, utilization, and storage (CCUS) techniques have been employed. These techniques are crucial to achieve a reduction of CO_2 emissions to the atmosphere, so that the increase in global average temperature does not exceed 2 °C above pre-industrial levels, as stated in the Paris Agreement (EDWARDS; CELIA, 2018). Among them, carbon dioxide utilization (CDU) represents a new economy for CO_2, since it can be used as feedstock in the synthesis of chemicals, fuels, and materials. The implementation of CDU techniques in high CO_2-generating sources, such as thermal power plants, can lead to near-zero carbon cycles, by integrating these sources with industrial processes (GALE et al., 2005).

According to Otto et al. (2015), only 0.36% of the global emissions of CO_2 have been used as feedstock for chemical production. Among the products, methanol is the most common, followed by carboxylic acids (formic acid and acetic acid), ethanol and higher alcohols, methylamines, hydrocarbons and methyl tert-butyl ether.

Carbon dioxide emissions may be reduced in two ways: directly and indirectly. The direct route consists of using CO_2 as feedstock in the synthesis of chemicals and the indirect route consists of using CO_2 as it is, in industries such as food and steel , in enhanced oil recovery, etc. Von de Assen, Jung and Bardow (2013) state that the indirect route has a higher potential of reducing CO_2 emissions than the direct route, but its quantification requires intensive efforts in computer simulations, and it is the focus of future research.

In this scenario, methane-reforming reactions are good candidates for CO_2 conversion. These reactions generate synthesis gas (syngas), a gas mixture containing primarily H_2 and CO, which is used as an intermediate to several other industrial processes, such as methanol synthesis, dimethyl-ether (DME) synthesis and Fischer-Tropsch processes (gas to liquids) (RAFIEE et al., 2018). Among the options of methane-reforming reactions, dry reforming of methane (DRM), bi-reforming of methane (BRM) and tri-reforming of methane (TRM) are viable alternatives.

Bi-reforming of methane has a few advantages over the other two: it is associated with less coke formation than DRM and it has a more easily manipulated H_2/CO ratio than TRM, which is achieved by manipulating feedstock composition (SINGH et al., 2018). Although being a combination of steam reforming of methane (SRM) (Eq. 1) and DRM (Eq.

2), BRM is widely reported to occur as depicted in Eq. 3 (KUMAR et al., 2016; OLAH et al., 2013; STROUD et al., 2018; TAHIR; TAHIR; AMIN, 2019).

SRM: $$CH_4 + H_2O \rightleftharpoons 3\,H_2 + CO \qquad \Delta H_{298K} = +206\ kJ/mol \qquad (1)$$

DRM: $$CH_4 + CO_2 \rightleftharpoons 2\,H_2 + 2\,CO \qquad \Delta H_{298K} = +247\ kJ/mol \qquad (2)$$

BRM: $$3\,CH_4 + 2\,H_2O + CO_2 \rightleftharpoons 8\,H_2 + 4\,CO \qquad \Delta H_{298K} = +220\ kJ/mol \qquad (3)$$

The produced syngas can be sold as a final product or used as feedstock for other processes. Ammonia, a highly commercial commodity, can be synthesized from the H_2 contained in syngas mixtures. In turn, its main use is for fertilizer production (in the form of urea or nitrates), which accounts for approximately 90% of the world's ammonia production (INSTITUTE FOR SUSTAINABLE PROCESS TECHNOLOGY, 2017).

In this scenario, different process configurations can be proposed in order to achieve both power plant-generated CO_2 abatement and fertilizer production. This work aims to propose an innovative process configuration to produce ammonia/urea and compare its relevant technical, economic, and environmental performance indicators with the ones from the conventional route for urea synthesis.

2. OBJECTIVES

The main objective of this work is to propose an innovative industrial process to produce ammonia and urea and promote CO_2 abatement by chemically converting CO_2 from a power plant flue gas.

The specific objectives are:

- Thoroughly evaluate the feasibility and applicability of the BRM process;
- Propose an alternative configuration to the ammonia and urea processes;
- Perform sensitivity analysis on operational parameters, such as bi-reforming feed, temperature, and pressure;
- Compare the proposed configuration with the conventional industrial process, with respect to their technical, economic, and environmental indicators;
- Carry out economic analysis for different scenarios other than the base case.

3. BACKGROUND

According to Rostrup-Nielsen (2000), hydrogen and syngas production via hydrocarbons will play a key role in the 21st century, especially for gas to liquid plants and hydrogen plants for refineries.

Currently, about 50 million tons of H_2 are produced globally every year. About 65% of the produced H_2 is consumed by the chemical sector (63% for ammonia and methanol synthesis and 2% for liquid hydrocarbons and higher alcohols synthesis) and about 30% is consumed by the refining sector (hydrotreating and hydrocracking of petrochemicals) (VOZNIUK et al., 2019).

Syngas can be generated from any carbon-based feedstock, such as biomass, coal, coke, and natural gas. The lowest cost routes, however, are the ones based on natural gas (WILHELM et al., 2001). In this scenario, SRM plays an important role, as it is the most used process for that matter (VOZNIUK et al., 2019).

3.1. STEAM REFORMING OF METHANE

Steam reforming of methane is an endothermic catalytic reaction where steam and methane are reacted in order to produce syngas with a H_2/CO ratio of 3 (Eq. 1), which is desired for processes that require high amounts of H_2. A conventional steam reformer (SR) comprises of hundreds of fixed-bed reactor tubes filled with catalysts and heated up by an external furnace. Although high temperatures (> 600 °C) and low pressures favor product formation, pressures of 20 to 30 bar are employed industrially for economic reasons. Outlet temperatures are in the range of 800 to 870 °C, with tube wall temperatures reaching up to 920 °C (VOZNIUK et al., 2019). Aasberg-Petersen et al. (2001) report new high-alloy tube materials being used in new plant designs, which can tolerate wall temperatures up to 1050 °C.

Catalysts used in SRM generally have nickel as the active metal, with varying supports. Common supports for SRM include α- and γ-Al_2O_3, MgO, $MgAl_2O_4$, SiO_2, ZrO_2 and TiO_2. These supports are associated with good porosity (meaning sufficient contact-times between reactants and catalyst), high reactivity, high resistance to sintering and high coke resistance of the metal particles. Other reported active metals include Ru, Rh, Pd, Ir and Pt, but they are very rarely used in industrial practice due to their expensiveness. Nickel, however

cheaper, is the less active of them and it is more prone to deactivation by coke formation or oxidation (VAN BEURDEN, 2004).

One of the drawbacks of reforming processes is the coke formation (also known as carbon depositing or carbon laydown). Among the reforming reactions, SRM is the one less prone to coke formation. This issue is responsible for catalyst deactivation due to fouling of the surface of the active phase, pellet destruction and plugging of catalyst pores. These coke deposits can cause tube erosion and/or plugging, leading to reactor shutdowns and high process maintenance costs (BARTHOLOMEW; FARRAUTO, 2006). Therefore, careful catalyst selection and reaction conditions, along with efficient reactor design, must be employed to avoid this issue.

As seen in Eqs. 4 to 6, coke formation tends to occur at higher temperatures, usually through Eq. 4. According to Carlsson (2015), Eq. 4 is favored at temperatures above 620 °C, and it is reversible when CH_4 is used as feedstock, but not when heavier hydrocarbons are used.

$$CH_4 \rightleftharpoons C + 2\,H_2 \qquad \Delta H_{298K} = +75\ kJ/mol \tag{4}$$

$$2\,CO \rightleftharpoons CO_2 + C \qquad \Delta H_{298K} = -172\ kJ/mol \tag{5}$$

$$CO + H_2 \rightleftharpoons C + H_2O \qquad \Delta H_{298K} = -131\ kJ/mol \tag{6}$$

One of the techniques employed to avoid coke formation is operating on elevated H_2O/CH_4 inlet ratios. Instead of a stoichiometric ratio of 1, common industrial practice operates on ratios of around 3 (CARLSSON, 2015) in order to increase CH_4 conversion (Eq. 1) and, therefore, reduce coke formation through Eq. 4. Excess of steam also suppresses coke formation by chemically interacting with the surface of the catalyst (BARTHOLOMEW; FARRAUTO, 2006).

Another reaction that also takes place in SRM processes is the water-gas shift (WGS) reaction (Eq. 7). Due to its exothermic nature, WGS is thermodynamically favored at lower temperatures and it is unaffected by pressure changes. In an SR, despite operating at high temperatures, WGS is favored over its reverse reaction (RWGS) due to the excess of steam present in the feed. Equilibrium for the WGS reaction can be pushed in either forward or reverse directions, depending on reaction conditions (PAL et al., 2018).

WGS: $$CO + H_2O \rightleftharpoons CO_2 + H_2 \qquad \Delta H_{298K} = -41\ kJ/mol$$ 7

The WGS reaction (or the RWGS) can be employed to change the H_2/CO ratio of the generated syngas. In this case, a dedicated WGS/RWGS reactor can be used right after the reforming process. Depending on the desired H_2/CO ratio, operating conditions and catalysts are specifically chosen to greatly favor either WGS or RWGS over the other one. In this case, WGS can be operated in two different ways: (a) temperatures between 190 and 250 °C on Cu-ZnO based catalysts (low temperature shift); or (b) temperatures between 350 and 450 °C on Fe_2O_3-Cr_2O_3 based catalysts (high temperature shift) (RATNASAMY; WAGNER, 2009). Although much less common than the WGS process, the RWGS process is operated at temperatures over 600 °C, with higher temperatures enhancing kinetics to the point that the reaction proceeds rapidly without the presence of a heterogeneous catalyst (BUSTAMANTE et al., 2004).

3.2. DRY REFORMING OF METHANE

Dry reforming of methane (Eq. 2) is an endothermic reaction that gets entropy-driven at high temperatures, and becomes thermodynamically favorable at temperatures above 920 K (VERNON et al., 1992). According to Kim et al. (2015), DRM is the best choice for efficient CO_2 utilization, but its use is extremely limited due to severe coke formation on the catalyst bed and process equipment.

Catalysts used in SRM are shown to be as active as for DRM. In comparison to nickel, which is the golden standard for SRM, noble metals such as Rh, Ru and Pt have higher stability, higher activity above 750 °C and higher coking resistance, but these catalysts are not generally considered for DRM due to their high costs (ASHIK et al., 2018; HALMANN; MEYER, 1998). On the other hand, non-noble metals have higher catalytic activity than noble metals, but also have a higher rate of carbon deposition (ASHIK et al., 2018).

Current research has been focused on developing catalysts with high activity, high stability and, mostly, high resistance to coke formation. Promotion of CO_2 dissociation results in more surface oxygen for reaction with carbon, which reduces coke formation. This can be achieved by adding alkali and alkaline-earth metal dopants, such as K, Na, MgO and CaO or by adding lanthanide/actinide dopants, such as UO_2, U_3O_8 and La_2O_3 to the catalyst. Poisons and alloy-forming components can also be added for greater coke resistance, however Pb, Sb,

Bi, Cu, Pt and Co were associated with extremely reduced activities (YORK; SUHARTANTO; GREEN, 1998). Ashik et al. (2018) report that nanoparticle catalysts show advanced catalytic activity and stability when compared to conventional catalysts.

Despite having similar thermodynamics to SRM, there are no reports of commercial plants operating pure DRM processes. There are, however, two reported processes that are based on DRM: the CALCOR process from Caloric, GmbH and the SPARG (Sulfur Passivated Reforming) process from Haldor Topsøe (GUNARDSON, 1997).

The CALCOR process was designed to generate high purity CO through DRM. While DRM yields a H_2/CO syngas ratio of 1, the CALCOR process yields 0.42. The process is very similar to a high-temperature reforming process, except that it operates at a very low pressure to reduce the reforming severity (GUNARDSON, 1997). It uses either a low-temperature process or a semi-permeable membrane for CO purification, achieving a low CH_4 slip of 0.0005% (TEUNER; NEUMANN; VON LINDE, 2001). The catalysts used in the reforming tubes are undisclosed, but are thought to be at last partially based on noble metals.

The SPARG process is remarkably similar to SRM, except that part of the steam is substituted by CO_2. It yields a syngas with a H_2/CO ratio ranging from 0.6 to 1.9. The principle behind this process is to prevent coke formation by using a "controlled poisoning" of the Ni catalyst, where a controlled amount of H_2S is constantly injected in the process stream to block carbon-forming sites in the catalyst (SONG; GUO, 2006). A pre-reformer is also featured in this process, in order to convert high hydrocarbons in the natural gas feed and avoid their cracking under low steam-to-carbon ratios associated with the process (GUNARDSON, 1997).

3.3. BI-REFORMING OF METHANE

The BRM is an endothermic reaction (Eq. 3) that comprises of SRM and DRM altogether. Similar catalysts from these methane reforming processes are also used in BRM. Although being slightly more endothermic than SRM, BRM also shares the same thermodynamics as the other reforming reactions (QIN; LAPSZEWICZ; JIANG, 1996). The main difference is that BRM produces a H_2/CO syngas ratio of 2, which is ideal for Fischer-Tropsch synthesis and methanol synthesis. This leads to a reduction in capital and operational expenditures, since less unit operations are required to achieve the desired syngas composition.

Just like DRM, BRM also has the potential of promoting CO_2 abatement. However, there are no reports of commercial plants operating pure BRM processes. Some methane-reforming plants, though, do operate SRM processes with a small rate of CO_2 in the feed (like the aforementioned SPARG process). It could be said that these plants operate BRM processes, but the amount of CO_2 fed is generally very small when compared to H_2O, unlike the stoichiometric H_2O/CO_2 ratio of 2 for pure BRM. Therefore, this work will consider as "BRM" only reforming processes operating at least near the stoichiometric ratio of Eq. 3.

Operational issues associated with BRM are nearly the same as with other reforming processes. Because it operates on a higher steam-to-carbon ratio, BRM is associated with more coke formation issues than SRM, but less than DRM, due to the presence of steam. Therefore, coke formation is still one of the drawbacks that limit the commercial application of this technology. Thus, just like as with DRM, research is focused on developing catalysts with higher stability, activity and resistance to coke formation (KUMAR; SHOJAEE; SPIVEY, 2015).

Another viable option for syngas production is the partial oxidation of methane (POM), which also produces syngas with a H_2/CO ratio of 2. Lately, POM has been drawing attention because of its highly exothermic nature, but it has some downsides associated with its industrial use. Some of them are: danger of explosions, formation of hot spots (which, in turn, might cause catalyst deactivation) and issues regarding the controlling of the reaction (LI et al., 2015b).

3.4. AMMONIA SYNTHESIS

Ammonia can be used as feedstock in many different industries, such as for the manufacture of explosives, hydrazines, amines, amides, nitriles and other organic nitrogen compounds that can be used as intermediates for dyes and pharmaceuticals (APPL, 2007a). The main use of ammonia, however, is for fertilizer production, which accounts for approximately 88% of the United States' domestic production. In 2017, approximately 150 million tons of ammonia were produced worldwide, with an expected increase of 8% in global capacity for the next 4 years (UNITED STATES GEOLOGICAL SURVEY, 2018).

The breakthrough in industrial ammonia synthesis happened in 1913, when Fritz Haber and Carl Bosch developed an industrial process to synthesize ammonia from its

elements. The "Haber-Bosch process" consisted in reacting H_2 and N_2 in stoichiometric rates inside of a reactor containing an iron oxide catalyst (and small quantities of cerium and chromium) at 550 °C and a pressure of around 2940 psi (20.3 MPa), according to Eq. 8 (SPEIGHT, 2002). Due to the nature of the reaction, ammonia must be removed from the system to shift the equilibrium to the right, which is done by condensing it and recycling unreacted H_2 and N_2 back to the reactor. The conversion per pass is estimated at 20 – 30% (TAVARES; MONTEIRO; MAINIER, 2013).

$$N_2 + 3\,H_2 \rightleftharpoons 2\,NH_3 \qquad \Delta H_{298K} = -46\,kJ/mol \tag{8}$$

Due to the exothermic nature of the ammonia synthesis reaction and the low per-pass conversion in the reactor, sequential catalyst beds coupled with internal heat exchangers can be used to achieve higher yields. Using this approach, a near-optimum profile of reaction rate versus temperature can be obtained by removing heat from the inlet of each bed, either by using waste heat boilers or by preheating reactor feed gas. This, in turn, increases steam production and reduces fuel consumption (FLÓREZ-ORREGO; DE OLIVEIRA JUNIOR, 2017).

Nitrogen feedstock for ammonia synthesis can be abundantly obtained from the air. Hydrogen, however, is obtainable through three main routes: gasification of coal, partial oxidation of heavy oil or waste oil and steam reforming of natural gas or other light hydrocarbons (naphtha, natural gas liquids) (TAVARES; MONTEIRO; MAINIER, 2013). The route applied in the process depends on geographical and economic circumstances, with the natural gas route being the most used, accounting for 85% of the world ammonia production (EUROPEAN FERTILIZER MANUFACTURERS' ASSOCIATION, 2000), 95% of capacity in North America and 86% of capacity in the European Union. China, on the other hand, has 66% of its ammonia production based on coal (APPL, 2007b).

Regardless of the chosen route for H_2 generation, CO_x is an inevitable side-product. Such carbon oxides (alongside O_2, H_2O and sulfur compounds) are responsible for the poisoning of iron catalysts, even when present in trace amounts. Thus, extensive purification of H_2 is need, which makes up for a significant fraction of the overall cost for ammonia production (KYRIAKOU et al., 2017).

Most of the catalysts used in ammonia plants are based on iron catalysts promoted with non-reducible oxides. In general, ammonia catalysts contain varying quantities of the

oxides of Al, Ca, K, Mg and Si as promoters (APPL, 2012). Catalysts based on Ru have also been reported. Despite being highly active, Ru catalysts face some challenges that prevent their widespread use in industrial processes. Its expensiveness is the main reason. Methanation of the carbon material used as a carrier in Ru catalysts is another one, which leads to decreased number of active sites and reduced overall life of the catalyst (LIU, 2014). According to data from Liu (2014), only 16 ammonia plants worldwide had Ru as their catalyst for ammonia synthesis from 1992 to 2010.

Ammonia production is responsible for over 1% of global energy-related CO_2 emissions every year, which accounts for about 420 million tons of CO_2. Most ammonia plants are designed to operate 330 days a year, with capacities ranging from 300,000 to 600,000 t/y, with some up to 1 Mt/y. On average, these plants emit over 1.6 t CO_2/t NH_3 when natural gas is used as feedstock, 2.5 t CO_2/t NH_3 with naphtha, 3.0 t CO_2/t NH_3 with heavy oil fuel and 3.8 t CO_2/t NH_3 with coal. If integrated with a urea plant, up to 40% of the produced CO_2 may be captured for use in urea synthesis (INTERNATIONAL ENERGY ASSOCIATION, 2017).

3.5. UREA SYNTHESIS

More than 90% of the urea globally produced is used as fertilizer (EDRISI; MANSOORI; DABIR, 2016). This is because urea has a high nitrogen content (46%), low cost and it is easy to handle and transport (AZEEM et al., 2014).

Urea was synthesized for the first time in 1828, by reacting cyanic acid and ammonia. Its industrial scale production, however, started in the early 1900's through cyanamide ($CNNH_3$) hydration, which was obtained from calcium cyanamide ($CaCN_2$), H_2O and CO_2. The development of the Haber-Bosch process in 1913 made urea synthesis through ammonia and CO_2 possible, especially because such process produces both necessary reactants. As for today, urea is exclusively produced by this method (MAXWELL, 2005).

The synthesis of urea ($(NH_2)_2CO$) consists of two reactions, depicted in Eq. 9 and Eq. 10. In Eq. 9, ammonium carbamate (NH_2COONH_4) is produced by reacting ammonia and CO_2, which decomposes to urea and H_2O in the next step (Eq. 10). However, biuret ($C_2H_5N_3O_2$) can also be produced, according to Eq. 11. Biuret is an undesirable product, as it is toxic to plants. To avoid this, excess of ammonia is used to favor ammonium carbamate production. Urea can also decompose to isocyanic acid (HNCO) and ammonia, as shown in

Eq. 12. This can also be avoided by using excess of ammonia in the process (MEESSEN, 2014).

$$2\,NH_3 + CO_2 \rightleftharpoons NH_2COONH_4 \qquad \Delta H_{298K} = -117\,kJ/mol \tag{9}$$

$$NH_2COONH_4 \rightleftharpoons (NH_2)_2CO + H_2O \qquad \Delta H_{298K} = +16\,kJ/mol \tag{10}$$

$$2\,(NH_2)_2CO \rightleftharpoons C_2H_5N_3O_2 + NH_3 \tag{11}$$

$$(NH_2)_2CO \rightleftharpoons HNCO + NH_3 \tag{12}$$

The ammonium carbamate intermediate is known to be extremely corrosive under certain conditions, which includes the ones generally used for urea production (170 to 200 °C and 150 to 200 bar). Other factors that increase corrosiveness are sulfur and oxygen content in the CO_2 used for synthesis (WAES, 1950).

4. LITERATURE REVIEW

This chapter reviews the recent advances in BRM, ammonia and urea processes, as well as in process integration. Since ammonia and urea processes are more than a half-century old, their focus will be on industrial changes of the process. Reaction mechanisms are not included due to it not being the scope of this work.

4.1. BI-REFORMING OF METHANE

Since there are no reports of commercial plants operating pure BRM process, it is impossible to develop a commercial overview of the state-of-the-art for such process. However, the Chiyoda Corporation in Japan reports a novel catalyst based on noble metals for a process named "CO_2-reforming" (CHIYODA CORPORATION, 2017). Although the name suggests a DRM process, it is more closely related to a BRM process due to the presence of steam in the feed. Researchers from the Chiyoda Corporation published a conference proceeding detailing the referred catalyst performance on a pilot plant test. According to them, syngas with a H_2/CO ratio of 2 (which further contributes to the theory of a BRM process) was generated at a rate of 400 Nm^3/h, with varying temperatures of 865 to 895 °C, pressures of 15 to 19 bar and a $CH_4/H_2O/CO_2$ feed molar ratio of 1.0/1.15~1.64/0.4~0.6. Stable operation was achieved for around 7,000 hours with less than 0.1wt% carbon deposition on the catalyst (MIKURIYA; YAGI; SHIMURA, 2008).

Most of BRM research is focused on catalyst performance and stability, since coke formation is one of the main issues. Stroud et al. (2018) evaluated the activity of Sn addition to Ni-based catalysts in the dry and bi-reforming of methane. Different Sn loadings were used in Ni-Sn/Al_2O_3 and Ni-Sn/CeO_2-Al_2O_3 catalysts, and their activity was measured in different temperatures and space velocities. The authors found that Ni-Sn/CeO_2-Al_2O_3 not only showed good levels of conversions for dry reforming, but also exhibited stable conversions towards bi-reforming, reaching a stable H_2/CO product ratio. They also state that, despite the good results obtained, coke formation and sintering are still the main culprits regarding catalyst deactivation in both reactions.

As mentioned by Li et al. (2015a), Ni/MgO catalysts have been studied intensively for reforming reactions due to its positive characteristics against coke formation.

According to the authors, the Lewis basic sites in such catalysts might be responsible for promoting the chemisorption of CO_2, which accelerates the reaction of CO_2 and deposited coke species, leading to increased catalyst stability.

Olah et al. (2013) tested the performance of a NiO/MgO catalyst for the bi-reforming of methane from any source. For this, the reaction was performed in a tubular reactor with temperatures varying from 800 to 950 °C and pressures from 5 to 30 atm. In conclusion, the authors reported constant syngas production with a H_2/CO molar ratio of 2, and also constant conversions of CO_2 and CH_4 for extended periods (over 300 h on-stream), hinting that coke formation might be low with such catalyst. The authors also report a single-pass conversion of 70 – 75% at 7 atm, which can be further increased to 80 – 85% by adjusting the H_2O/CO_2 inlet ratio.

Photocatalytic BRM is another approach found in the literature. Tahir, Tahir & Amin (2019) tested silver-nanoparticles supported over protonated graphitic-carbon nitride (Ag/pg-C_3N_4) nanosheets for stimulating H_2O and CO_2 reduction to fuels in different reforming processes. Different Ag-loadings into the catalyst samples were tested in steam reforming of methane, dry reforming and bi-reforming with a single-step methanol production. The authors claim that photocatalytic bi-reforming is the most promising approach for methanol, CO and H_2 generation in a single step.

Besides natural gas, other sources of CH_4 have also been under research for BRM. Schiaroli et al. (2019) compared the performance of Ni-based catalyst promoted by Rh on DRM and BRM tests, with clean biogas (an equimolar mixture of CH_4 and CO_2) as feedstock. The authors found out that adding small amounts of Rh were enough to significantly reduce coke formation, and that BRM is associated with less coke deposition than DRM, due to the presence of steam. They also found out that, out of all the tested supports for the catalyst, MgO had greater stability and resistance to coke formation.

4.2. AMMONIA SYNTHESIS

Recent studies on ammonia synthesis mainly focus on reducing energy consumption per tonne of ammonia produced, reducing operational temperature and pressure requirements in the synthesis loop, better catalyst understanding and sustainable pathways for industrial production.

Schlögl (2003) points out that the Haber-Bosch process as it is today has been studied and optimized since its development in the 1910's, and that any other proposal of alternative routes for ammonia synthesis would require intensive research to meet the high standards of the "conventional" routes. The author also mentions that improvements in ammonia synthesis (such as higher-efficiency catalysts that would account for lower pressure requirements) would also need intensive research, since the current process has efficiencies of up to 70% and most of the losses come from the synthesis of the precursors, i.e. from SRM and hydrogen purification.

Flórez-Orrego and De Oliveira Junior (2016, 2017) presented two papers on an exergy approach to optimize a 1,000 MTPD (metric tonnes per day) ammonia plant based on steam reforming. In the first one, the authors claim that 59% of the total exergy destruction rate (136.5 MW) takes place at the reforming process, and that the overall exergy efficiency of the ammonia plant is 66.36%, which is enhanced by using a purge gas treatment process. The authors also claim that total and non-renewable exergy costs lie around 1.7950 kJ per unit of exergy (kJ) of ammonia produced and that CO_2 emissions of the produced ammonia lie around 0.0881 kg_{CO2}/MJ_{NH3}. In the second paper, the authors compared a base-case and the optimized operating conditions to note that the performance of each component and their interdependencies are key factors for optimal ammonia loop design, even on near-optimum reactor operation, where higher reaction rates are achieved and lower catalyst volumes are required. The authors also claim that the refrigeration system and the ammonia converter represent more than 71 – 82% of the total exergy destruction in the ammonia synthesis, which was found to be 38.8 MW for the base-case operations and 25.6 MW for the optimized design.

One of the approaches for a simpler ammonia production is the electrochemical synthesis. Kyriakou et al. (2017) present a very concise state-of-the-art in this matter, highlighting key aspects of such approach for ammonia synthesis. The authors note that such approach has been limited to laboratory scale and has been studied for less than 20 years. It also worth noting that different factors influence the reaction rate, when compared to the conventional Haber-Bosch process (such as the applied potential and the generated current). The authors also compile dozens of reported results from other authors, showing that electrochemical synthesis of ammonia is possible in three different ranges of temperature: high (over 500 °C), intermediate (between 100 and 500 °C) and low (less than 100 °C). Based on these results, the authors conclude that further research is needed in the fields of materials

science, heterogeneous catalysis and solid state ionics in order to develop a possible industrial process.

Li et al. (2016) apply a proton-assisted electron transfer pathway to promote solar ammonia synthesis on a BiOCl catalyst. The study aims to overcome the kinetic inertia of N_2 by using oxygen vacancies, which allows for lower energy consumption. The authors state their findings were important to establish a truly catalytic system for solar ammonia synthesis, despite overall intrinsic mechanisms remaining unclear.

Frattini et al. (2016) simulate (via Aspen Plus) the integration of three different renewable energy systems into the ammonia process, in hopes to eliminate steam reforming as a source of hydrogen. These systems were biomass gasification, biogas reforming and water electrolysis with electricity from solar or wind energy. As for the results, the authors state that the use of any of the three options would not limit ammonia production, since all of them have nearly the same primary energy consumption as the conventional method via natural gas (14 – 15 kW/kg_{NH3}). However, GHG emissions are higher with biomass (3.59 and 3.82 kg_{CO2}/kg_{NH3}, respectively, for biogas and solid biomass) and virtually zero with water electrolysis, whereas natural gas values lie around 2.05 kg_{CO2}/kg_{NH3}.

4.3. UREA SYNTHESIS

Recent developments in industrial urea synthesis are mainly carried out by companies that provide technology licenses for new plants, such as Casale SA, Maire Tecnimont SpA, Montedison SpA, Saipem SpA and Toyo Engineering Corporation. Research is generally focused on reducing energy consumption, reducing plant height and reducing corrosion in plant equipment, due to the presence of ammonium carbamate (MEESSEN, 2012).

Saipem SpA, in partnership with Sandvik, developed Safurex®, a high-alloy duplex (austenitic-ferritic) stainless steel capable of withstanding the corrosive environments present in urea processes. Safurex® can be used in nearly all equipments associated with urea plants, such as stripper tubes, pool reactor and condenser tubes, high-pressure piping, scrubbers, lining, reactor trays and high-pressure valves (SANDVIK, 2017).

Other reported changes to urea processes include: the Urea 2000plus® process, which uses a series of pool reactors for capacities up to 2,500 MTPD and pool condensers for capacities between 2,500 and 5,000 MTPD (STAMICARBON B.V., 2017); the Avancore®

process, which combines the Urea 2000plus® process and the Safurex® technologies into a single process operating on a ground-level reactor (which makes maintenance easier) (MURZIN, 2015).

The Avancore® process was first licensed in 2010 for Tierra del Fuego Energia y Química S.A. in Rio Grande, Argentina, in a 2,700 MTPD ammonia and urea plant (STAMICARBON B.V., 2012).

5. PROCESS CHARACTERISTICS

This section presents a brief description of both the conventional and the innovative processes, so as to highlight their main differences and similarities.

Both processes, starting from their feedstocks up to the ammonia synthesis section, have the same goal: generate a mixture of H_2 and N_2 that is pure enough not to poison the ammonia synthesis catalyst and with as few inert components as possible (i.e. Ar and CH_4). These must be achieved using the minimum amount possible of feedstocks (mainly NG) and utilities (i.e. thermal and electric power).

In the ammonia synthesis section, the goal is to convert as much H_2 and N_2 into NH_3 as possible. This should be achieved using a high-efficiency chemical loop to avoid as much H_2 and N_2 losses as possible in the purge stream.

As for the urea synthesis section, the goal is to have as much NH_3 and CO_2 needed to produce a target of 2000 MTPD (metric tonnes per day) of urea. These reactant streams must be in predefined conditions, which vary according to the type of process selected for urea generation (e.g. CO_2 or NH_3-stripping processes). Due to the high complexity of urea processes, this work presents a detailed configuration up to the urea synthesis section. This section is represented solely by a conversion reactor, which was set to generate urea with a 98 mol% reactants conversion.

Both the amine scrubbing section and the ammonia synthesis loop section are the same for both configurations, equipment wise. The only differences are the operating conditions and equipment sizing, which will be covered in section 7.

5.1. THE CONVENTIONAL ROUTE

The conventional route for NH_3 production has the SRM as its core process. It uses natural gas, steam and air as their global inputs, and generates high-purity CO_2 and NH_3 as outputs, which are then directed to urea synthesis. The general layout of the process is shown in Figure 1.

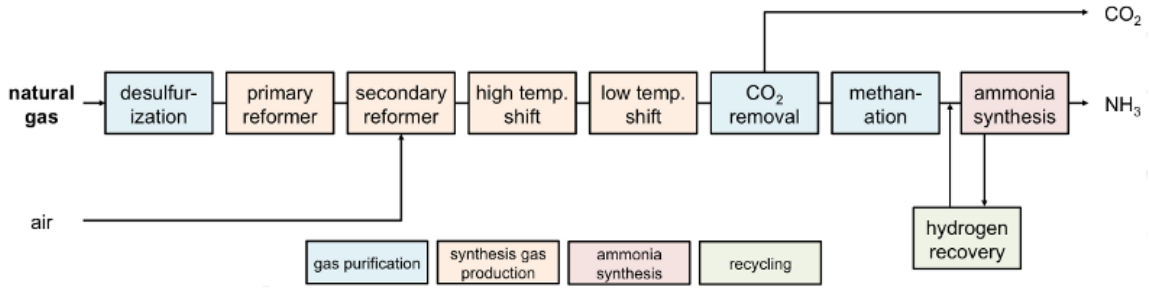

Figure 1 – Conventional configuration for ammonia synthesis via natural gas (Taken from Yuan (2014)).

The conventional route starts with NG being mixed with steam and then compressed to 20 - 30 bar. This mixture is heated to around 550 °C and passed on the steam reformer (SR) where SRM takes place, generating H_2 and CO. Process gas exits at around 900 °C and is directed to the secondary reformer, where it is then mixed with compressed pretreated air, which provides enough N_2 to reach a 3:1 ratio of H_2 to N_2 when the process gas is ready for ammonia synthesis. Air also provides O_2 to convert residual hydrocarbons from NG left in the process gas. The outlet stream of the secondary reformer, where combustion reactions take place, can reach temperatures as high as 1300 °C.

After cooling, the process gas is passed on the high-temperature shift (HTS) reactor, cooled once again and then passed on the low-temperature shift (LTS) reactor. These shift converters are responsible for converting all produced CO into H_2 and CO_2 via the WGS reaction (Eq. 7). By now, only traces of CH_4 and CO are left in the process gas, which is further cooled to remove excess water. Then, amine scrubbing is carried out, removing up to 99.8 mol% of CO_2 in the process gas. The removed CO_2 is regenerated as another stream and directed to urea synthesis.

To avoid poisoning of the ammonia synthesis catalyst, all CO, CO_2 and H_2O must be removed from the process gas. Traces of CO and CO_2 in the process gas are removed in the next step – methanation – and residual H_2O is removed on a zeolite adsorption column. Process gas is then compressed to 120 - 300 bar in a multistage compressor with intercooling and directed to the ammonia synthesis loop.

At the beginning of the synthesis loop, process gas is mixed with recycled H_2, and N_2 and is then directed to the ammonia reactor. The exiting process gas is cooled, so that ammonia condenses, and it can be separated from the gases, which are redirected to synthesis (recycle). A purge stream is used to avoid the buildup of inert components, i.e. CH_4 and Ar.

Liquid ammonia is then directed to the urea reactor, together with CO_2 regenerated in the amine scrubbing step. Since CO_2 is the limiting reactant in this process, excess liquid NH_3 is sold as a byproduct stream.

5.2. THE INNOVATIVE ROUTE

The innovative route is based on BRM. Its main advantages in relation to the conventional route is the removal of all 4 reactors used for process gas purification, absence of the secondary reformer, lower operating pressures and high potential for CO_2 abatement. The general layout is shown in Figure 2.

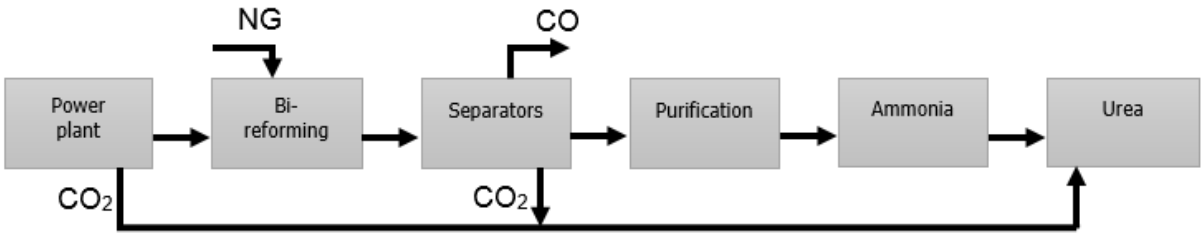

Figure 2 – Innovative configuration for ammonia and urea synthesis.

This route starts with NG being heated and then mixed with the flue gas from the power plant, which contains only CO_2 and H_2O (an oxy-fuel power plant is considered). This mixture is compressed to 10 bar and mixed with excess steam to maintain a 3:3:1 molar ratio of CH_4:H_2O:CO_2. This process gas is heated and then passed on the bi-reformer (BR) where BRM takes place. Process gas exits at around 850 °C, and it is cooled to remove excess water and then directed to the same amine scrubbing step of the conventional route.

Another cooling step takes place to remove water and the process gas is directed to the pressure swing adsorption (PSA) section. The exiting process gas consists mainly of 99.9999 mol% of H_2 and the remaining components exit in a separate stream (rich in CO) that is sold as byproduct.

Process gas consisting almost entirely of H_2 is mixed with enough external N_2 so that a H_2/N_2 ratio of 3 is reached. Multistage compression, loop synthesis, purge stream and ammonia flashing are carried in the same way as the conventional route, with the only exception being a reduced purge percentage, due to the low content of inert gases, since N_2

comes with only 0.01 mol% Ar impurities and no methanation occurs to produce CH_4 in the process gas.

To complete the urea synthesis, CO_2 regenerated from the amine scrubbing step is mixed with extra CO_2 coming from the power plant flue gas, so that enough CO_2 is directed to urea synthesis and all NH_3 is converted into urea.

5.3. AMINE SCRUBBING SECTION

The main objective of this section is to remove as much CO_2 as possible from the process gas and then regenerate such CO_2 as a separate stream. This is achieved by using aqueous solutions of alkylamines as absorvents, which are countercurrently reacted with the process gas.

The amine scrubbing section, as seen in Figure 3, consists of two main columns: the absorber and the stripper. In the first step, process gas flows upwards the absorber while the amine solution flows downwards, absorbing CO_2 along the way. The amine solution saturated with CO_2 is called “rich solvent” or “rich amine”, and it is sent to a reboiled-stripper column. Heat from the reboiler is used to regenerate the amine solution (“lean solvent” or “lean amine”) that is recycled to the absorber, while CO_2 is desorbed and exits the stripper in the overhead gas. Excess water is removed from the overhead gas and sent back to the stripper, while high-purity CO_2 is obtained afterwards.

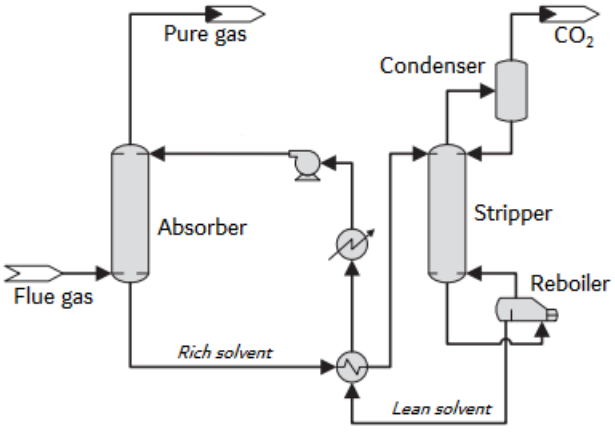

Figure 3 – Process flow diagram for the amine scrubbing process (adapted from Sutanto et al. (2017)).

5.4. AMMONIA REACTOR

The ammonia reaction is relatively simple, with no side reactions and no products instability. The reaction, however, is highly exothermic (Eq. 8), which requires a cooling system to obtain high degrees of conversion (KHADEMI; SABBAGHI, 2017). One of the many possible ways to achieve such cooling is by using a quench reactor, as depicted in Figure 4.

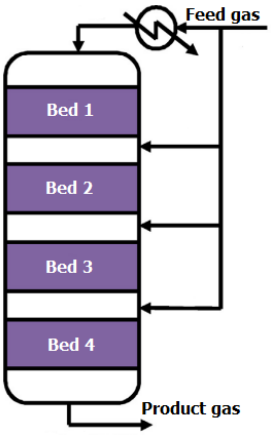

Figure 4 – Adiabatic quench reactor with 4 catalyst beds (adapted from Khademi and Sabbaghi (2017)).

Apart from the ammonia reactor, the ammonia synthesis loop comprises of 3 main elements: the reactor, a cooler and a flash separator. After being compressed, process gas (a mixture of H_2 and N_2) is sent to the quench reactor, where NH_3 formation takes place. The reactor outlet is then cooled so liquid NH_3 can be separated in a flash separator. Liquid NH_3 exits the ammonia synthesis section while unreacted gases are recycled to the reactor. A purge stream is necessary to avoid the buildup of inert gases.

6. METHODS AND MODELING

This chapter presents the detailed rationale behind the modeling of both configurations, as well as the relevant data for the simulation. All process simulations were carried out on Aspen Plus® v10 software by Aspen Tech, using Peng-Robinson equation of state, as it is recommended for systems containing hydrocarbons, air, water and combustion gases. Moreover, the referred equation of state not only has a large applicability range in terms of pressure and temperature, but also a large binary interaction parameter database (ÖZKARA-AYDINOĞLU, 2010; PENG; ROBINSON, 1976).

To evaluate the feasibility of the bi-reforming process, a thermodynamic analysis was carried out to select the initial operating conditions for the bi-reformer i.e. the base case. Other possible configurations are presented varying some of the operating parameters.

As for the whole BRM process, a base case encompassing the whole configuration was also created. For this, several assumptions based on literature reviews and data were used. Once the base case was properly established, technical, economic and environmental indicators were used to compare both processes, and an economic analysis was carried out to determine how different economic scenarios might affect such indicators for both processes.

6.1. BI-REFORMING CONDITIONS

The thermodynamic analysis to select the parameters for the base case of the bi-reformer was performed using a Gibbs reactor (RGibbs) from Aspen Plus. These parameters were temperature, pressure and inlet molar ratio of reactants.

Aspen Plus's Gibbs reactor simulates outlet compositions in the reactor for given inlet compositions and operational parameters. This is done by applying the Gibbs free energy minimization technique, which is based on the assumption that a system at its minimum value of Gibbs energy is a thermodynamically favorable system (ÖZKARA-AYDINOĞLU, 2010).

For the thermodynamic analysis, six different species were considered: CH_4, CO_2, H_2O, H_2, CO and C(s). C(s) corresponds to the solid carbon formation (coke deposition) that might occur in the catalyst bed.

The total Gibbs energy of a system (G^{tot}) is given by the sum of the chemical potential of all components:

$$G^{tot} = \sum_{i=1}^{N} n_i \mu_i \quad (13)$$

Where n_i is the number of moles of the component *i*, μ_i is its chemical potential and N is the total number of components in the system. The chemical potential of species *i* is defined as:

$$\mu_i = \Delta G_{fi}^0 + RT \ln\left(y_i \hat{\varphi}_i \frac{P}{P_0}\right) \quad (14)$$

Where ΔG^0_{fi} is the standard Gibbs energy of formation of species *i*, R is the molar gas constant, T is the absolute temperature, y_i is the mole fraction of species *i*, $\hat{\varphi}_i$ is the fugacity coefficient calculated using the aforementioned equation of state, P is the operating pressure and P_0 is the standard pressure. Substituting both equations and adding a term to account for the formation of solid carbon, we get:

$$G^{tot} = \sum_{i=1}^{N} \left[n_i \Delta G_{fi}^0 + n_i RT \ln\left(y_i \hat{\varphi}_i \frac{P}{P_0}\right)\right] + n_c \Delta G_{fC(s)}^0 \quad (15)$$

Where n_c is the number of moles of deposited solid carbon.

Minimization of Eq. 15 for a given temperature-pressure-feed provides the thermodynamic equilibrium composition of each species in the reactor. These compositions do not depend on the reaction network, therefore, nothing else but inlet stream characteristics and reactor temperature and pressure must be specified (ÖZKARA-AYDINOĞLU, 2010).

For a better evaluation of the reaction in view of the reactants, some parameters were used to evaluate preliminary results. They are: CH_4 conversion (Eq. 16), CO_2 conversion (Eq. 17), H_2O conversion (Eq. 18), H_2 yield (Eq. 19) and coke yield (Eq. 20). It is worth noting that the yield adopted takes into account the number of atoms present in the molecules of either reactants and products, i.e. H_2 yield is based on the number of hydrogen atoms in the desired product (H_2) and its possible sources from reactants (H_2O and CH_4). The same rationale is used for coke yield, but based on carbon atoms.

$$X_{CH4} = \frac{F_{CH4,in} - F_{CH4,out}}{F_{CH4,in}} \times 100 \quad (16)$$

$$X_{CO2} = \frac{F_{CO2,in} - F_{CO2,out}}{F_{CO2,in}} \times 100 \quad (17)$$

$$X_{H2O} = \frac{F_{H2O,in} - F_{H2O,out}}{F_{H2O,in}} \times 100 \quad (18)$$

$$Y_{H2} = \frac{2\,F_{H2,out}}{2\,F_{H2O,in} + 4\,F_{CH4,in}} \times 100 \quad (19)$$

$$Y_{Cs} = \frac{F_{Cs,out}}{F_{CO2,in} + F_{CH4,in}} \times 100 \quad (20)$$

Where X_i is the molar conversion of species *i*, $F_{i,in}$ is the inlet molar flow of species *i*, $F_{i,out}$ is the outlet molar flow of species *i* and Y_i is the yield of species *i*.

6.2. KINETIC MODELS

To achieve a more realistic modeling of the processes, kinetic models were incorporated on Aspen Plus.

All the selected kinetic models consist of a Langmuir-Hinshelwood-Hougen-Watson (LHHW) model, which considers both the adsorption and desorption steps over the catalyst surface, and derived rate equations can be used more accurately outside the experimental range. The model also assumes isothermal operation within the catalyst. Aspen Plus has a built-in option for LHHW kinetics. For this, rate equations must have the setup depicted in Eq. 21.

$$r = \frac{(kinetic\ factor)(driving\ force\ expression)}{(adsorption\ term)} \quad (21)$$

6.2.1. Reforming sections and methanation

Kinetic models for the bi-reforming process as a whole are scarce on the literature. Kim et al. (2015) reported a power-law kinetic model of 1.35 to 1.39th-order in

relation to methane-only over $Ni/La/Al_2O_3$ catalysts. Although showing good results, the referred kinetic model was found to be too simplistic and another approach was chosen.

For the BRM simulation, most authors use a combination of kinetic models, generally comprising of a model for DRM, a model for SRM and a model for WGS. Usually, models based on catalysts of the same active element are used (mainly nickel), although catalyst supports might differ.

Based on this approach, individual models were gathered and analyzed in order to find which ones were best. However, BRM, DRM, MET, SRM, and WGS reactions are nothing but a linear combination of each other (e.g. subtracting WGS from SRM gives DRM; adding up SRM and WGS gives MET, etc.). To select a reasonable set of independent reactions, the matrix reduction method (MRM) proposed by Missen and Smith (1998) was applied.

The MRM uses atomic conservation, the representation of chemical species by a molecular formula, and the solution of sets of simple linear algebraic equations. The method relates the number of species and the number of different atoms in a closed system, in order to obtain a "proper set" of independent chemical equations. A "proper set" of chemical equations must have the property of yielding any other chemical equation by adding or subtracting multiples of the members of this set.

Applying the MRM, the proper set of chemical equations consists of 2 independent reactions. Among all possible reactions, the SRM and WGS reactions were chosen to represent the many subsystems in both the conventional and innovative configurations, as there are extensive studies available in the literature regarding these reactions.

It is important to note that, since both BRM and SRM take place on a nickel catalyst and have the same species involved, the same set of independent reactions take place on both reformers, even in different operating conditions. The same is true for the MET section, which also operates on nickel catalysts.

For SRM and WGS reactions, the kinetic model from Xu and Froment (1989a) seems to be the best choice, as it was used by many authors, even in operating conditions outside of the established in the original model, yielding good results.

The model proposed by Xu and Froment (1989a) consists of three rate equations, each one for a separate reaction: SRM, WGS, and MET (Eqs. 22 to 24, respectively). The model was developed over a $Ni/MgAl_2O_4$-spinel catalyst, at temperatures ranging from 573 to 848 K and pressures from 3 to 10 bar. The authors recognize that such operating temperatures

are below industrial practice, but this was a necessary step to avoid measuring only equilibrium conversions. Feed conditions used for SRM were either 3 or 5 (in H_2O/CH_4 ratio) with a fixed H_2/CH_4 molar ratio of 1.25. For WGS and MET, the H_2/CO_2 molar feed ratio was either 0.5 or 1. As mentioned before, only the reaction rates of SRM and WGS were taken into consideration, i.e. reaction rate of MET (Eq. 24) was ignored.

$$r_{SRM} = \frac{k_{SMR}}{p_{H2}^{2.5}}\left(p_{CH4}p_{H2O} - \frac{p_{H2}^{3}p_{CO}}{K_{SMR}}\right)(DEN)^{-2} \quad (22)$$

$$r_{WGS} = \frac{k_{WGS}}{p_{H2}}\left(p_{CO}p_{H2O} - \frac{p_{H2}p_{CO2}}{K_{WGS}}\right)(DEN)^{-2} \quad (23)$$

$$r_{MET} = \frac{k_{MET}}{p_{H2}^{3.5}}\left(p_{CH4}p_{H2O}^{2} - \frac{p_{H2}^{4}p_{CO2}}{K_{MET}}\right)(DEN)^{-2} \quad (24)$$

$$DEN = 1 + K_{CO}p_{CO} + K_{H2}p_{H2} + K_{CH4}p_{CH4} + \frac{K_{H2O}p_{H2O}}{p_{H2}} \quad (25)$$

Where r_{SRM}, r_{WGS}, and r_{MET} represent the reaction rates of SRM, WGS, and MET; p_{CH4}, p_{H2O}, p_{CO}, p_{CO2}, and p_{H2} represent the partial pressures of methane, water, carbon monoxide, carbon dioxide, and hydrogen, respectively; k_{SRM}, k_{WGS}, and k_{MET} are reaction rate constants; K_{SRM}, K_{WGS}, and K_{MET} are chemical equilibrium constants; and K_{CH4}, K_{H2O}, K_{CO}, and K_{H2} are adsorption constants.

Since the literature lacks both experimental data and kinetic models for BRM, the selected kinetic model was validated using the experimental data from Jun et al. (2011).

The authors, however, do not present the equations for the chemical equilibrium constants. Therefore, the equations from Rahimpour, Arab Aboosadi and Jahanmiri (2012) were used, as depicted in Eqs. 26 and 27.

$$K_{SMR} = exp\left(30.114 - \frac{26830}{T}\right) \quad (26)$$

$$K_{WGS} = exp\left(-4.036 + \frac{4400}{T}\right) \quad (27)$$

6.2.2. Secondary reformer

In the secondary reformer (SDR), O_2 is added and unconverted CH_4 undergoes a combustion reaction. Since combustion reactions are fast (kinetically speaking) and reach nearly 100% conversion, no kinetic models were considered for the secondary reformer. Instead, all O_2 added was considered to react with the components inside the reformer (mainly CH_4).

6.2.3. Shift converters

As for the shift converters, Rase (1977) proposed a single kinetic model suitable for both HTS and LTS. This model already accounts for diffusional resistances (further detailed in section 6.3) and, according to Rajesh et al. (2001), it is by far the most successful in predicting the kinetics of industrial shift converters. The experimental data for the HTS were obtained for a chromia-promoted iron oxide catalyst while the LTS used a copper-zinc oxide catalyst. This model is valid for temperatures in the range of 149 to 483 °C and no specifications for pressure were given, although the author states that it is valid for pressures above 24.8 atm. It is important to note that these models have different rate equations than the one previously selected for the WGS reaction (Eq. 23). This happens due to the different catalysts used in each case, in order to avoid SRM taking place both in the HTS and LTS reactors. The rate equation is depicted in Eq. 28.

$$r_g = 0.00423 \psi_g k_g \left(y_{CO} y_{H2O} - \frac{y_{CO2} y_{H2}}{K_g} \right) \qquad 28$$

Where ψ_g is the activity factor; k_g is the rate constant; K_g is the equilibrium constant and y_i is the mole fraction of species *i* (i = CO, H_2O, CO_2, and H_2). The subscript *g* refers to the reaction in question (g = HTS and LTS).

6.2.4. Ammonia synthesis

Nielsen, Kjaer and Hansen (1964) proposed a kinetic model for the ammonia synthesis reaction (ASR), which was developed using conditions close to industrial practice. All their experiments were carried out on a commercial KM-I-R pre-reduced promoted iron catalyst, which is essentially a triply promoted catalyst based on K_2O-CaO-Al_2O_3. The model is valid for temperatures in the range from 370 to 495 °C, pressures in the range from 150 to 310 atm, and H_2/N_2 ratios from 1.15 to 6.23. The rate equation is shown in Eq. 29.

$$r_{ASR} = \frac{k_2^0 (K_a^2 a_{N2} - a_{NH3}^2 / a_{H2}^3)}{[1 + K_3 a_{NH3} / a_{H2}^w]^{2\alpha}} \quad 29$$

Where $k^0{}_2$, $K^2{}_a$ and K_3 are reaction rate constants; a_i is the activity of species *i* (i = N_2, H_2 and NH_3); w and α are constants determined experimentally.

6.3. EFFECTIVENESS FACTORS

The selected kinetic models, except the one used in the shift converters, were derived from laboratory-scale experimental data, where catalyst particles are generally small and/or high linear velocity flows are used. In these scenarios, transport processes hardly restrict the measured reaction rate. In an industrial context, however, one of the most important transfer processes is the diffusion inside the catalyst pore system, which is usually negligible in laboratory reactors. If the reaction rate is fast compared to mass and/or heat transfer, the overall reaction rate of the particle will be affected, due to the resulting concentration and temperature gradients between particle center and bulk gas (AIKA et al., 1995).

To compensate for these unaccounted diffusion effects, effectiveness factors are frequently used in computational simulations. They are defined as the observed overall reaction rate (i.e. inside the catalyst pellet) divided by the theoretical reaction rate if the entire catalyst pellet was kept at the external surface i.e. diffusion effects are very fast, presenting no limitation to the mass transfer (ALBERTON et al., 2009). For a reaction *j*, the effectiveness factor (η_j) is given by Eq. 30.

$$\eta_j = \frac{\int_0^{V_P} r_j(p_i, T)\,dV}{r_j(p_{i,S}, T_S)\,V_P} \qquad 30$$

Where V_p is the volume of the catalytic pellet; r_j is the reaction rate for reaction *j;* p_i is the partial pressure of species *i* inside the catalyst pellet; T is the temperature inside the catalyst pellet; $p_{i,S}$ is the partial pressure of species *i* at the surface of the pellet; and T_S is the temperature at the surface of the pellet.

In tubular reactors and reformers, the effectiveness factor varies according to the temperature and the position inside the reactor, since it depends on both real and theoretical reaction rates and such reaction rates also vary throughout a tubular reactor. In the literature, expressions for effectiveness factors for different reactions, catalysts, tube characteristics, etc. can be found. For the sake of simplicity, fixed values of effectiveness factors were used, as listed in Table 1.

Table 1 – Values of effectiveness factors for the selected kinetic models.

	SRM	**WGS**	**HTS**	**LTS**	**ASR**
Effectiveness factor	0.07[a]	0.70[a]	1.00[b]	1.00[b]	0.80[c]

([a]): Taken from De Groote and Froment (1996);
([b]): This kinetic model was developed industrially, therefore no effectiveness factor is needed;
([c]): Taken from Nielsen, Kjaer and Hansen (1964).

6.4. PROCESS DESIGN AND SIMULATION

Process design was carried out individually for each process, considering the peculiarities of each one. The conventional route was operated at 28 bar, while the innovative route operates at 10 bar (as justified in section 7.1).

Following the technology readiness level (TRL) guidelines of the European Union Framework Programme for Research and Innovation, the TRL of all processes in the conventional route is 9 (maximum), since not much have changed since its first development in the early 1900's. As for the innovative route, the amine scrubbing step, the ammonia synthesis loop and the urea synthesis section are the same as in the conventional route, except for different equipment sizing. Therefore, their TRL is also 9. The PSA section of the innovative route is also 9, since it is a mature technology and its use in newer ammonia plants have been increasing over the last decades (AIKA et al., 1995; SIRCAR; GOLDEN, 2000).

The BRM process, however, has an estimated TRL of 3, according to research from the University of Southern California (UNITED STATES DEPARTMENT OF ENERGY, 2012).

The simulation was carried out with the following assumptions:

- Natural gas composition was considered to be 100% methane;
- No pressure drops across piping and equipment;
- The power plant is considered to operate on oxy-fuel (i.e. its flue gas consists of only CO_2 and H_2O);
- Both reformers had an inlet temperature of 550 °C and outlet temperature of 850 °C (as justified in section 7.1);
- Operating conditions of equivalent equipment in both processes were kept as close as possible from each other (e.g. as mentioned above, both reformers had the same inlet and outlet temperature to make comparison "fair" enough);
- Cooling equipment had a maximum possible temperature of 30 °C for both configurations, so external cooling is not needed;
- Any heating above 250 °C was carried out in fired heaters operating on NG;
- Compressors had an isentropic efficiency of 72%;
- The cooling duty requirements for the four-stage compressor were not considered;
- All reactors (excluding the urea reactor) were modeled as single-tube adiabatic plug-flow reactors;
- Both reformers were modeled as multitube plug-flow reactors with the same external constant heat flux.

6.5. PROCESS UTILITIES

The utilities were: electricity, low-pressure steam (LPS), medium-pressure steam (MPS), high-pressure steam (HPS), fired heater (FH), low-pressure steam generation (LPSg), medium-pressure steam generation (MPSg), high-pressure steam generation (HPSg) and cooling water (CW), as shown in Table 2.

The fired heater was considered to operate with methane, and its price was taken from the U.S. Energy Information Administration website (EIA, 2020). Prices for the other utilities were taken from Aspen Plus's internal database. The CO_2 emission factors were taken

from the U.S. Environmental Protection Agency rule E9-5711, named "Mandatory Reporting of Greenhouse Gases" (EPA, 2009). This rule applies to all sectors of the U.S. economy, whether it is a fossil fuel supplier or a direct greenhouse gas emitter.

It is important to note that negative values of prices and CO_2 emissions, for some of the cold utilities, indicate selling of the utility and a CO_2 emission credit for avoiding the use of fossil fuels to generate such utilities.

Table 2 – Utilities breakdown.

	T_{in} (°C)	**T_{out} (°C)**	**Inlet vapor fraction**	**Outlet vapor fraction**	**Pressure (bar)**	**Heating or cooling value (GJ/tonne)**	**Price ($/GJ)**	**CO_2 emission factor (tonne/GJ)**
Electricity							21.53*	0.0964
Hot								
LPS	125	124	1	0	2.3	2.19	1.90	0.0658
MPS	175	174	1	0	8.9	2.03	2.20	0.0658
HPS	250	249	1	0	39.8	1.72	2.50	0.0658
FH	-	-	-	-	-	50.03	4.06	0.0559
Cold								
LPSg	124	125	0	1	2.3	-2.19	-1.89	-0.0658
MPSg	174	175	0	1	8.9	-2.03	-2.19	-0.0658
HPSg	249	250	0	1	39.8	-1.72	-2.49	-0.0658
CW	20	25	0	0	1.0	-0.02	0.212	0

(*): equivalent to 0.0775 $/kWh.

6.6. ECONOMIC METRICS

Equipment costs were estimated using the CAPCOST v. 2012 software and methodology provided by Turton et al., 2018. The following considerations were applied in equipment pricing:

- A nationalization factor of 1.4 for Brazil was applied to all equipment costs, as proposed by Machado et al. (2018);
- The maximum operating pressure for all equipment was defined as 10% above the required operating pressure, to compensate for possible pressure fluctuations;
- Reactors in the conventional configuration were modeled as horizontal pressure vessels;
- Flash separators were modeled as vertical pressure vessels;
- Amine stripper reboilers were modeled as kettle reboiler heat exchangers;

- The secondary reformer was modeled as a pyrolysis furnace;
- SRM and BRM reformers were modeled as reactive fired-heat reformers;
- Mixers, splitters, and valves were not priced;
- Catalysts and MEA requirements were not priced due to their very low impact on final costs;
- Project life was of 15 years, with 2 years of construction;
- An annual interest rate of 10% was considered;
- Due to the complexity of the urea synthesis section, its components and reactors were not priced.

As for the economic indicators, the methodology thoroughly described in Turton et al. (2018) was used to evaluate the cost of manufacture for each process and to perform a cash flow analysis. To do so, one of the main variables is the revenue from sales and raw materials costs. The prices for all raw materials and products for both configurations are shown in Table 3.

With all relevant data gathered, the cash flow analysis was carried out, still using the CAPCOST v. 2012 software. The chosen relevant economic indicator was the net present value (NPV). This indicator is widely used in the business and financial scenarios, and its detailed information can be easily found in the related literature.

Table 3 – Price breakdown for all raw materials and products from both configurations.

	Classification	**Price ($/tonne)**	**Reference**
Urea	Product	246.00*	IHS Markit (2020a)
Ammonia	Product	250.00*	IHS Markit (2020b)
CO-rich stream	Product	70.65×	-
Natural Gas	Raw material	202.90*	EIA (2020)
Air	Raw material	56.60	Ulrich and Vasudevan (2006)
Water	Raw material	4.42	Ulrich and Vasudevan (2006)
External N_2	Raw material	76.06	Humphreys (2011)
CO_2 from power plant	Raw material	60.00	CPLC (2017)

(*): Annual average prices for 2019;
(×): The rationale behind this pricing will be justified in Section 7.7.

6.7. TECHNICAL METRICS

A few technical metrics were chosen to be evaluated for each configuration. The selected metrics were proposed by Araújo et al. (2015), and they are simple metrics that describe some parameters of a process, mainly to support decision-making. These technical metrics require minimum computational effort, and they are defined in a way that the smallest the value, the better the performance.

- Energy factor (E-factor): unit mass of raw materials per unit mass of products, minus 1;
- Electric energy intensity (EEI): unit of electric energy per unit mass of products;
- Thermal energy intensity (TEI): unit of thermal energy per unit mass of products.

6.8. ENVIRONMENTAL METRICS

Just like the technical metrics described in section 6.7, the environmental metrics were also proposed by Araújo et al. (2015). The same description of the technical metrics applies to the environmental ones, keeping the rule of the smallest the value, the greener the process.

- Global carbon intensity (GCI): unit mass of outlet CO_2 minus unit mass of inlet CO_2 per unit mass of products;
- Electric carbon intensity (ECI): unit mass of outlet CO_2 minus unit mass of inlet CO_2 per unit energy of required electricity;
- Thermal carbon intensity (TCI): unit mass of outlet CO_2 minus unit mass of inlet CO_2 per unit energy of required thermal energy.

It is important to note that the conventional route does not have any inlet CO_2, only output CO_2 from the utilities. The innovative route, however, has both the inlet CO_2 to the bi-reformer and the outlet CO_2 from the utilities.

6.9. ECONOMIC ANALYSIS

The economic analysis was carried out by varying some of the prices for raw materials and products, and then reassessing the previously selected economic metric for each configuration for comparison. As an example, annual average prices of previous years were used for some of the involved materials to get the break-even point for each configuration.

7. RESULTS AND DISCUSSIONS

In this chapter, the results obtained by the modeling previously described and by the resulting simulation are reported. After every reported result, a discussion is given.

7.1. THERMODYNAMIC ANALYSIS

For the first part of the analysis, different feed compositions were evaluated at different temperatures and a pressure of 1 bar. This part aimed to evaluate whether hydrogen production is possible through BRM or not and how it behaves to temperature changes. For this, 10 different runs were performed, each one with varying inlet CH_4:H_2O:CO_2 molar ratios as shown in Figure 5.

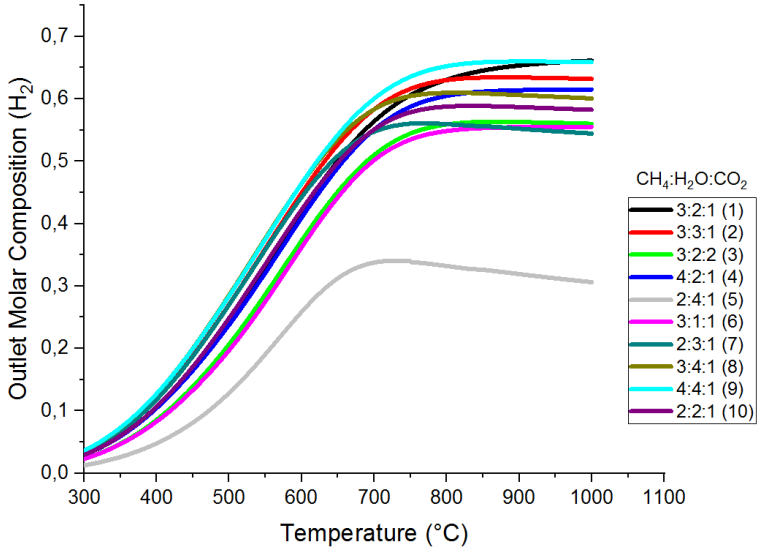

Figure 5 – Hydrogen molar composition in the outlet stream of the Gibbs reactor for varying temperatures and CH_4:H_2O:CO_2 molar feed ratios at a pressure of 1 bar.

Figure 5 shows that H_2 production is indeed viable from BRM. For all 10 runs, increasing temperatures between the range of 400 and 700 °C are associated with increased H_2 production. Both reforming reactions and the WGS reaction occur at these temperatures. For most runs, peak production is achieved between 800 and 850 °C, and a plateau is established. At temperatures higher than 850 °C, runs 2, 3, 5, 7, 8 and 10 display a decrease in H_2 output. The reason behind this is that high temperatures favor the RWGS reaction rather

than the WGS, due to the endothermicity nature of the former, which starts to consume H_2 at a slightly higher rate than the production obtained from the reforming reactions. In this scenario, CH_4 has become the limiting reactant and H_2 production via both reforming reactions is diminished.

Figure 6 shows the results of CH_4 conversion, H_2O conversion, CO_2 conversion and H_2 yield.

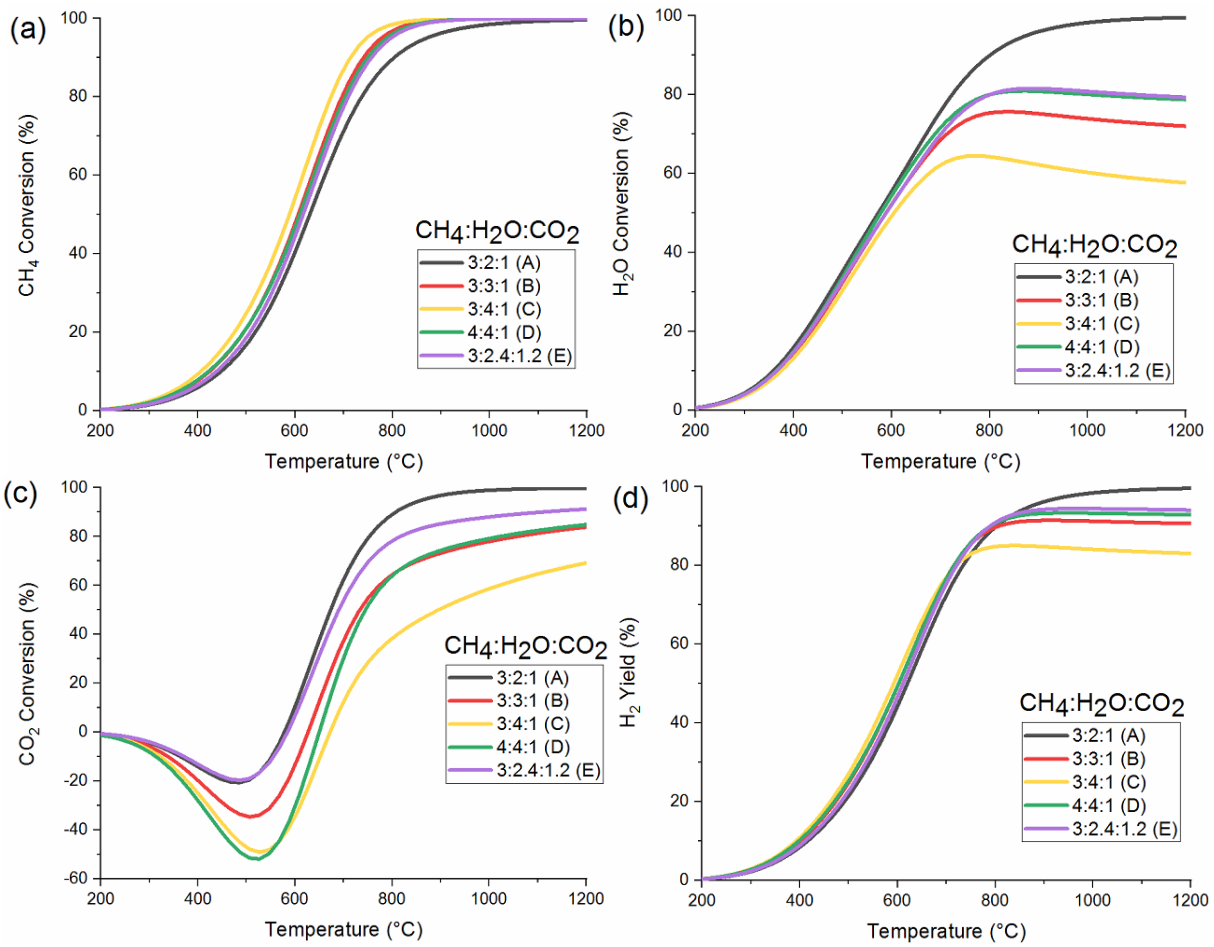

Figure 6 – (a) CH_4 conversion, (b) CO_2 conversion, (c) H_2O conversion, (d) H_2 yield over a range of temperatures from 200 to 1200 °C, 1 bar, and varying feed molar ratios.

Figure 6a shows that CH_4 conversion increases with increasing temperature, since it is a reactant to both endothermic reforming reactions. At temperatures around 800 °C, for runs B to E, almost 100% conversion is achieved due to two main reasons: 1- these setups have a higher water content, which favors SRM; 2- SRM is also favored due to its slightly lower energy requirement when compared to DRM. In such cases, CH_4 acts as the limiting reactant.

As for H_2O conversion (Figure 6b), the effects of CH_4 limitation are clearly observed. At the temperature in which CH_4 reaches 100% conversion or at higher temperatures, H_2O conversions start to decrease, since SRM is halted and RWGS starts generating H_2O by consuming H_2 and CO_2. This is also verified by inspecting Figure 6c: CO_2 conversions do not decrease even after CH_4 is totally consumed, which corroborates to the fact that it is consumed in the RWGS reaction.

Also in Figure 6c, it is observed negative values for CO_2 conversion at temperatures between 200 and 550 °C, which suggests CO_2 formation. The exothermic WGS reaction is favored at such temperatures, which leads to CO_2 formation by consuming H_2O and CO. However, at temperatures higher than 550 °C, RWGS becomes predominant over WGS and DRM also starts taking place, which leads to positive values of CO_2 conversion.

From Figure 6d, H_2 yield has a decreasing trend once CH_4 becomes the limiting reactant due to the rate of RWGS becoming greater than the rate of H_2 formation through either reforming reactions, as mentioned beforehand.

As for coke formation, Figure 7 shows that coke yield is negligible. According to Trimm (1997), higher temperatures are associated with higher rates of coke formation, which are well represented in Fig. 5. Despite having low values of carbon deposition throughout all analyzed temperatures, it is observed an increasing trend at temperatures around 1050 °C. Since operating temperatures usually do not exceed 920 °C, this increasing trend is not of much concern.

From this analysis, run A has better rates of CO_2 conversion and H_2 yield, which are the main desired objectives at this point. However, excess steam is generally desired in the feed stream to avoid coke formation. Therefore, run B was chosen as the starting feeding ratio for the simulation.

7.2. BI-REFORMING KINETIC MODEL VALIDATION

For the BRM kinetic model validation, data from Jun et al. (2011) were used. The authors analyzed CH_4 and CO_2 conversions by performing 17 runs with varying feed compositions, temperature, pressure, and gas hourly space velocity (GHSV). For their experimental data collection, a 10 mm internal diameter and 30 mm length isothermal reactor was used, with 0.45 g of Ni-CeO/$MgAl_2O_4$ as catalyst, in a Ni/Ce/oxide fixed weight ratio of

12/4/84. Table 4 displays the cases used by the authors, which were the same ones used for validation.

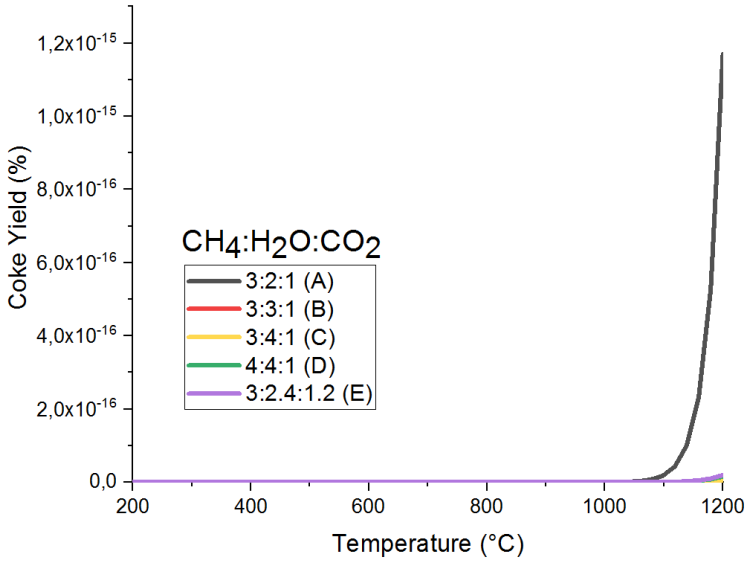

Figure 7 – Coke yield over a range of temperatures from 200 to 1200 °C, 1 bar, and varying feed molar ratios.

Table 4 – Experimental conditions used for the kinetic model validation

Case	**Temperature (°C)**	**Pressure (atm)**	**GHSV ($ml_{CH4}/(g_{cat}·h)$)**	**Mole ratio ($CH_4/H_2O/CO_2/N_2$)**	**Inert fraction***	**Remarks**
1	750	10	5000	3/3/1.2/3	0	Equilibrium
2	800	10	5000	3/3/1.2/3	0	
3	850	10	5000	3/3/1.2/3	0	
4	900	10	5000	3/3/1.2/3	0	
5	850	10	2500	3/3/1.2/3	0	
6	850	7.5	5000	3/3/1.2/3	0	
7	850	10	5000	3/3/1/3.2	0	
8	850	10	5000	3/2/1.2/4	0	
9	850	10	5000	3/4/1.2/2	0	
10	850	10	50000	3/3/1.2/3	0.97	Non-Equilibrium
11	850	10	100000	3/3/1.2/3	0.97	
12	850	10	200000	3/3/1.2/3	0.97	
13	850	10	400000	3/3/1.2/3	0.97	
14	750	10	50000	3/3/1.2/3	0.97	
15	750	10	100000	3/3/1.2/3	0.97	
16	750	10	200000	3/3/1.2/3	0.97	
17	750	10	400000	3/3/1.2/3	0.97	

(*): Inert fraction = catalyst/(catalyst + alumina ball). Source: Jun et al. (2011).

Cases containing inert fractions had their catalyst mass changed from 0.45 to 0.4365 g on Aspen Plus's setup tool to compensate for the alumina ball. Results obtained were reported in Figure 8.

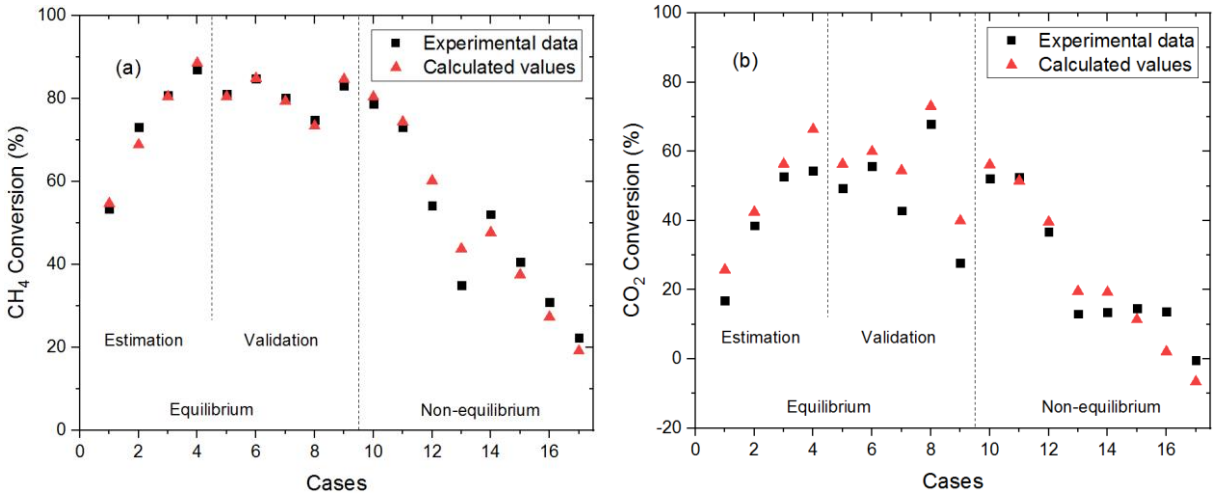

Figure 8 – Experimental data from Jun et al. (2011) and calculated values for (a) CH_4 conversion and (b) CO_2 conversion for each case described in Table 4.

As shown in Figure 8, values obtained by the kinetic model are very close to experimental data for cases 1 to 9, which represent equilibrium conversions. Most cases from 9 to 17 have modest similarities between experimental and predicted data. The slight discrepancy, however, might be due to catalyst differences. Although our approach is an approximation model due to the lack of kinetic models for BRM as a single process, the results obtained were satisfactory, especially at thermodynamic equilibrium. Additionally, BRM and SRM are very similar processes, and some authors report that near-equilibrium conversions are achieved in industrial SRM plants, which further validates the kinetic model used (CHIBANE; DJELLOULI, 2011; RAJESH et al., 2000).

From now on, effectiveness factors have been taken into account.

7.3. BI-REFORMING SIMULATION

With enough data gathered for the BRM process, it was possible to proceed with the simulation of the reactor. As mentioned previously, currently there are no reports of industrial plants in the world operating BRM processes. Therefore, a comparative basis was

unavailable. To counter this issue, missing parameters were adopted from conventional SRM plants. As for results analysis, conventional SRM was also taken as a basis.

Table 5 presents the initial assumptions for the base case. Since most plants operate at inlet temperatures of 550 °C and outlet temperatures of 850 °C, these values were adopted. However, reported inlet temperatures usually range from 400 to 600 °C and outlet temperatures usually range from 800 to 870 °C, up to a maximum of 920 °C due to material limitations (VOZNIUK et al., 2019).

Table 5 – Initial assumptions of the base case for the BRM reformer.

Parameter	**Value**
Reactor type	Plug-flow reactor [a]
Pressure	10 bar (no pressure drop inside the reformer)
Inlet temperature	550 °C
Outlet temperature	850 °C
External heat flux	100 kW/m^2 [b]
Molar feed ratio (CH_4:H_2O:CO_2)	3:3:1
Inlet molar flow	5.48 Mmol/h
Active phases	Vapor only
Catalyst	Ni (kinetic model does not depend on support)
Catalyst particle density	2355.2 kg/m^3 [c]
Reforming reactor bed voidage	0.528 [c]
Tube diameter	0.1018 m [c]
Tube length	12.0 m [c]
Number of tubes	363

([a]): Taken from Olah et al. (2013);
([b]): Taken from Quon (2012);
([c]): Taken from Xu & Froment (1989b).

Most industrial plants operate under pressures of 20 to 30 bar due to economic reasons and to avoid coke formation, even though lower pressures yield higher conversions of reactants (VOZNIUK et al., 2019). These values of pressures, however, are usually associated to high energy-demanding compressors. In an attempt to reduce energy consumption, a lower pressure of 10 bar was chosen as a starting point. Other viable configurations running on higher values of pressure are shown in Section 7.4.

Quon (2012) reports that tube diameters of 8 to 12 cm are ideal for SRM, as much as tube lengths of 8 to 10 m. Since most authors report diameters around 10 cm and tube lengths of 12 m (as seen in Table 5), these values were chosen.

Although the adopted kinetic model considers as important only the active phase of the catalyst (i.e. nickel), catalyst particle density and reforming reactor bed voidage data from a commercially used $Ni/MgAl_2O_4$ catalyst were used.

The number of tubes was calculated by having it as a “degree of freedom” while all other parameters were set on Aspen Plus. A simple sensitivity analysis was carried to obtain an approximation of how many tubes would be needed to achieve the desired values of H_2 in the outlet stream and to consume the lowest value possible of heat in the reformer. As a result, the value of 363 tubes was chosen.

Since the outlet temperature was set not to exceed 850 °C, equilibrium conversions of the reactants and product yields were calculated at that temperature and 10 bar. For comparison purposes, equilibrium conversions/yields are shown together with simulated conversions/yields in Table 6.

Table 6 – Simulated characteristics of inlet and outlet streams for the BRM reactor, as well as equilibrium data for comparison.

	Inlet	**Outlet**	**Conversion/Yield**	
			Calculated	**Equilibrium**
CH_4 molar flow (kmol/h)	2348.57	602.15	74.36	74.58
CO_2 molar flow (kmol/h)	782.86	388.83	50.33	50.78
H_2O molar flow (kmol/h)	2348.57	996.18	57.59	58.17
H_2 molar flow (kmol/h)	0	4845.24	68.77	69.11
CO molar flow (kmol/h)	0	2140.45	68.35	68.62
Total molar flow (kmol/h)	5480.00	8972.84		
Temperature (°C)	550.00	850.68		
Pressure (bar)	10			
Reformer duty (Gcal/h)	119.55			
Residence time (s)	1.20			

As expected, BRM also proceeds at near-equilibrium conversions, just like SRM. Data from commercially employed steam reformers were used to evaluate if 363 tubes are in an acceptable range within steam reforming plants, as displayed in Table 7. Since every plant operates on different setups, molar feed per tube was used as a comparative parameter.

As mentioned before, there is no current information on commercial plants operating BRM, therefore, a good comparison basis cannot be reached. At a first glance, it might seem that our simulated BRM was overdesigned, because of the low molar feed per tube. However, SRM plants operate with H_2O/CH_4 ratios greater than 3, which is far above the stoichiometric ratio of 1. This, in turn, leads to a great part of the steam in the reactor (almost 50% of the total inlet molar flow) acting only as an inert to avoid coke formation, to increase CH_4 conversion, and to favor the WGS reaction instead of the RWGS. The design presented herein, on the other hand, does not operate on heavy reactants excess, which corresponds to almost 6/7 of the feed being “reactive”. Roughly, it can be stated that if

conventional SRM running on the same level of "inlet flow reactiveness" as the process here proposed, molar feed flows of both processes would be nearly the same (1/2 of an average total feed of 23.34 kmol/h for SRM, totalizing 11.67 kmol/h *versus* 6/7 of a total feed of 15.096 kmol/h for BRM, totalizing 12.94 kmol/h).

Table 7 – Reported tube characteristics of commercial steam reformers.

	De Deken, Devos and Froment (2009)	**Soliman et al. (1988)**	**Soliman et al. (1988)**	**Xu and Froment (1989b)**	**This work**
Inlet temperature (°C)	520	450	454	520	550
Inlet pressure (bar)	28.1	36.5	34.8	29.0	10.1
H_2O/CH_4 feed ratio	3.3	4.4	4.3	3.4	1
Tube diameter (m)	0.102	0.1	0.0935	0.1016	0.1016
Tube length (m)	12	12	12	12	12
Number of tubes	1*	280	200	-	363
Total molar feed per tube (kmol/h)	24.084	23.271	21.663	24.335	15.096

(*): In this work, the authors analyzed a single tube taken from a reformer composed of 80 tubes.

Since the proposed design requires more heat duty to the reactor than the conventional SRM, an increased number of tubes is needed to properly accommodate the needed heat flux and safely operate outside tube material limitations.

Tonkovich et al. (2007) report that conventional steam reformers operate at residence times of the order of 1 s. For a steam reforming plant capacity of 450.000 Nm^3/day of H_2, Shah (2017) reports a residence time of 1 s. Although SRM and BRM have some differences, the obtained value of residence time seems to be within the expected range.

Results for molar composition profile, reactant conversion profiles, and temperature profile inside the reactor are shown in Figure 9. Right at the entrance of the reactor, a sharp behavior is observed. This also occurs in SRM, and it is due to reactants readily getting in contact with catalyst particles and at low product concentrations, which leads to rapid reactants consumption and heat consumption (i.e., sharp decreases in both temperature and reactants molar composition and sharp increases in reactants conversion and products molar composition).

The behavior of the conversion of the reactants is just the same as the one described in Section 7.1, and as seen in Figure 4a, Figure 4b, Figure 4c, and Figure 4d.

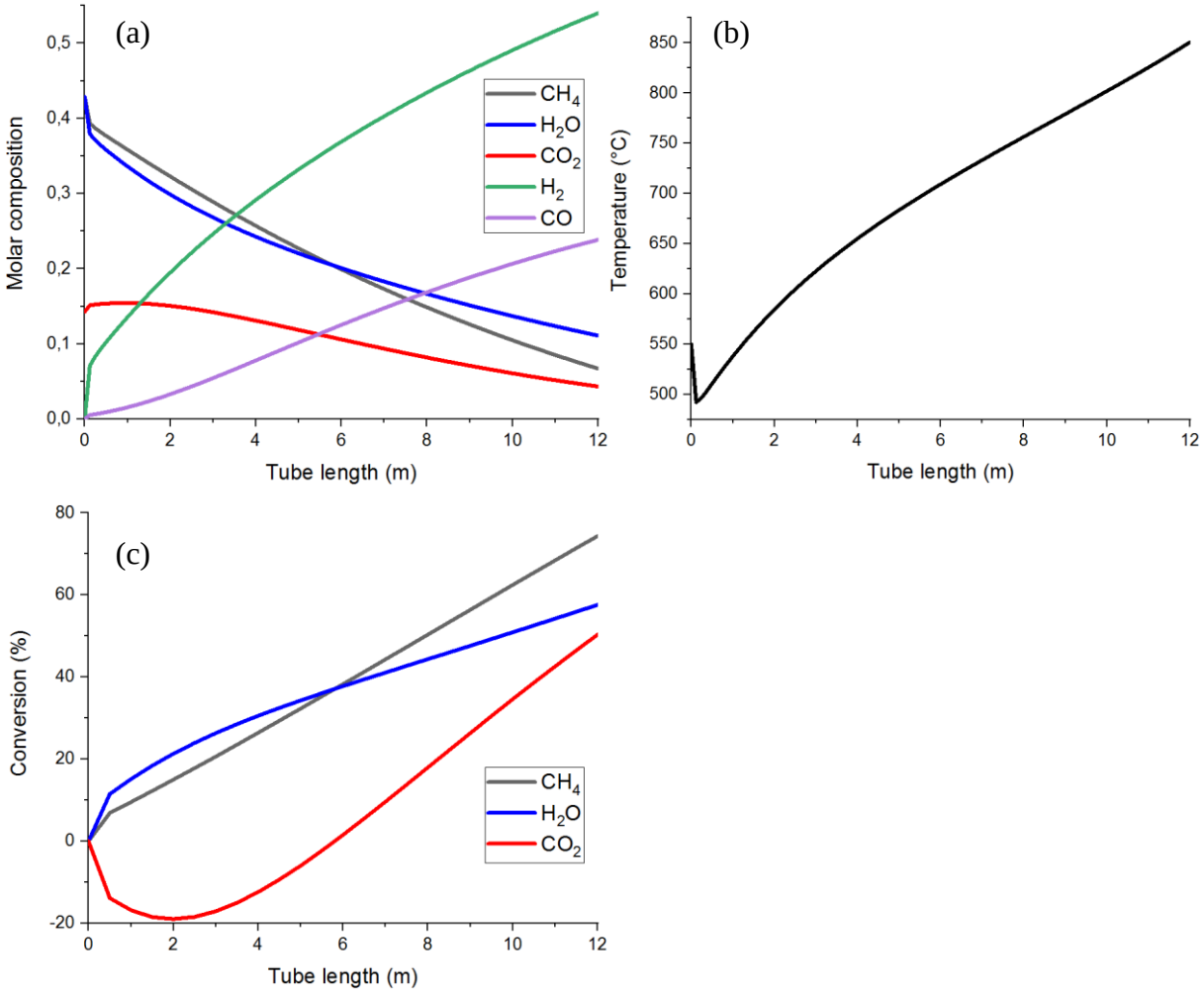

Figure 9 – Profiles of (a) molar composition, (b) temperature, and (c) reactants conversion inside the reactor.

7.4. BI-REFORMING SENSITIVITY ANALYSIS

In order to analyze other viable configurations for the BRM, sensitivity analyses were performed on 3 key aspects of reformer design: feed composition, pressure, and temperature. The results obtained are displayed on Tables 8, 9, and 10, respectively.

An important key factor of these analyses is the CO_2 conversion. For increasing values of pressure, increased values of temperature are also required in order to obtain the same (or a higher) CO_2 conversion. Although configurations operating at different temperatures are possible, they are generally not desirable due to either be near the maximum recommended operational value of 870 °C, or to decrease CO_2 conversions, which is not in accordance to the goal of this work.

To facilitate a comparison of the obtained results, the value for the outlet H_2 flow was fixed in order to generate enough H_2 for the next step. Although the minimum required amount of H_2 for ammonia synthesis is 4.68 Mmol/h (Table 3), values near to that obtained for the base case (4.845 Mmol/h) were adopted.

In industrial practice, residence times are key parameters for good process operation, as it defines the minimum amount of contact time between catalyst and reactants. Therefore, values of residence time were also fixed around 1 s whenever possible, in order to avoid either too low or too high feed stream velocity profiles.

Table 8 – Bi-reforming reactor characteristics for different pressures.

	Inlet pressure (bar)				
	1	**5**	**10 (base)**	**20**	**30**
T_{out} (°C)	672.16	789.71	850.68	920.17	964.86
Duty (Gcal/h)	99.86	113.37	119.55	126.88	131.49
Number of tubes	303	344	363	385	399
Inlet total feed (Mmol/h)	5.48	5.48	5.48	5.48	5.48
Outlet $\dot{F}_{H2}$ (kmol/h)	4843.2	4855.3	4845.2	4849.4	4853.1
CH_4 conversion (%)	71.26	73.66	74.36	75.23	75.72
CO_2 conversion (%)	22.66	42.71	50.33	57.60	61.53
H_2O conversion (%)	63.71	59.42	57.58	56.03	55.21
Residence time (s)	0.11	0.59	1.20	2.46	3.72

As seen in Table 8, higher values of pressure require longer contact times and higher temperatures. For configurations running at 20 and 30 bar, both values are beyond the operational standards (1 s and 870 °C, respectively). Additionally, higher pressures are also associated with the need of high-energy demanding compressors.

When forcing residence times to be around 1 s for all non-base configurations, several fixed parameters have their values violated. For the configuration running at 1 bar, more than 1700 tubes would be needed, which just seems a huge number, i.e. high reforming reactor volume and, consequently, plant space. For the 5 bar configuration, temperatures would exceed 1400 °C. For both the 20 and 30 bar configurations, the number of tubes would be less than 200, but CO_2 conversions would be lower than -10% and the required H_2 production would not be met.

Table 9 displays other viable configurations for different inlet characteristics. Steam reforming generally operates at a H_2O/CH_4 molar ratio of 3, since higher steam-to-carbon ratios are generally associated to less coke formation. To analyze the changes in BRM

outputs for different steam-to-carbon ratios (0.5, 0.75, 2, and 3) at a pressure of 10 bar, inlet total feed was increased in every different case.

Table 9 – Bi-reforming reactor characteristics for different inlet molar ratios at 10 bar.

	Inlet $CH_4/H_2O/CO_2$ molar ratio				
	3/2/1	**3/3/1 (base)**	**3/4/1**	**3/8/1**	**3/12/1**
T_{out} (°C)	849.55	850.68	850.04	850.28	849.09
Duty (Gcal/h)	122.84	119.55	115.93	106.05	104.73
Number of tubes	373	363	352	322	318
Inlet total feed (Mmol/h)	5.42	5.48	5.63	6.60	8.10
Outlet $\dot{F}_{H2}$ (kmol/h)	4677.0	4845.2	4887.5	4791.0	4810.1
CH_4 conversion (%)	65.05	74.36	80.84	93.79	97.54
CO_2 conversion (%)	67.51	57.83	33.07	-26.94	-72.33
H_2O conversion (%)	63.81	50.33	52.36	38.54	30.41
Outlet H_2/CO molar ratio	1.97	2.26	2.52	3.42	4.31
Residence time (s)	1.25	1.20	1.15	0.95	0.80

As steam content increases in the feed stream, CH_4 conversion increases as well as H_2/CO ratios, which implies that SRM is strongly favored over all other reactions, as seen in Table 9. Excess inlet steam reduces the "reactiveness" percentage of the feed stream, meaning that less heat of reaction must be supplied to each tube, but the number of tubes should increase to achieve the H_2 production demands. However, a decreasing trend in the number of tubes is observed due to: (a) excess steam favoring the WGS reaction (i.e. generating H_2), which can be confirmed by high negative values of CO_2 conversion and high values of H_2/CO ratio; (b) SRM being favored over DRM due to the excess steam and its lower endothermic nature; and (c) higher CH_4 conversion. Residence times were around 1 s order of magnitude.

Regarding the outlet temperature, an infinite number of configurations are viable, and an economic analysis is needed for a better assessment. Table 10 shows only a few examples of such viable configurations.

Generally, to keep residence times around 1 s, a lower number of tubes requires more inlet feed, due to less heat being supplied to the reformer, causing decreases in the conversions. The opposite is true for a higher number of tubes. This leads to a trade-off between capital expenditures (number of tubes) and operating expenses (amount of inlet CH_4), which requires a more detailed analysis in future steps.

Table 10 – Bi-reforming reactor characteristics for different outlet temperatures at 10 bar.

	Case			
	#1	**#2**	**#3**	**#4**
T_{out} (°C)	772.43	802.78	843.10	847.26
Duty (Gcal/h)	115.35	117.32	118.64	120.29
Tubes	350	356	360	365
Inlet total feed (Mmol/h)	7.29	6.43	5.57	5.57
Outlet $\dot{F}_{H2}$ (kmol/h)	4867.4	4857.7	4820.0	4878.6
CH_4 conversion (%)	54.61	62.65	72.63	73.59
CO_2 conversion (%)	23.87	34.87	48.10	49.34
H_2O conversion (%)	46.66	51.02	56.60	57.14
Outlet H_2/CO molar ratio	2.49	2.37	2.28	2.27
Residence time (s)	0.96	1.07	1.19	1.20

7.5. PROCESS DESIGN

Both configurations had some key aspects in common, as described in Section 6.4. Their process flow diagrams (PFD) were divided into sections, so equipment naming and process overview could be easier to grasp. Each section from both routes will be thoroughly described.

Equipment had their names assigned according to their role, route, section, and order inside such section, respectively. The generic formula is: A-BCD, where A is the equipment role (*C* for compressors; *D* for compressor drives; *E* for heat exchangers; *H* for fired heaters; *P* for pumps; *R* for reactors and reformers; *T* for towers; *V* for flash vessels), B is the route it belongs to (*X* for the conventional route and *Y* for the innovative route), C is the section the equipment belongs to (*1* to *6*, as will be shown in the subsequent subsections) and D is the order that it appears inside such section (e.g. equipment E-Y43 is a heat exchanger, in the innovative route, located in section 4 and it is the third heat exchanger from the section; equipment P-X11 is a pump, in the conventional route, located in section 1 and it is the first pump from the section).

Table 11 presents the specifications of all raw materials of both configurations.

Table 11 – Specifications for all inlets of both configurations.

	Natural Gas	Water	Flue Gas	Air	External N_2
Temp. (°C)	25	25	180	25	25
Pressure (bar)	4	2	4	1	10
Composition (mole fraction)					
CH_4	1.00				
H_2O		1.00	0.66		
CO_2			0.33		
O_2				0.28	
N_2				0.71	0.99
Ar				0.01	0.01

7.5.1. The conventional route

The process flow diagram for the conventional route is shown in Figure 10.

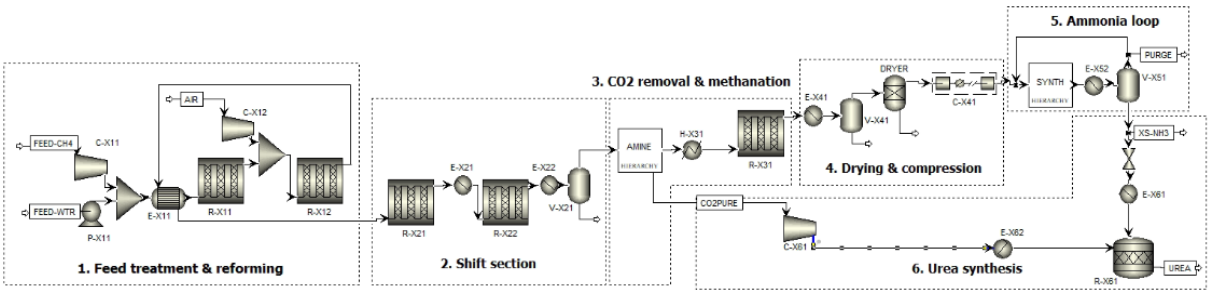

Figure 10 – Final PFD for the conventional route.

The first section, shown in detail in Figure 11, features the required feed treatment for the SRM process and the SRM itself. Natural gas (X01) is compressed to 28 bar and then mixed with water (X02) that was also pumped to 28 bar, to reach a H_2O to CH_4 ratio of 3. This mixture is heated to 550 °C in E-X11, by using the secondary reformer outlet stream as a hot stream, and then passed on the SR (R-X11). The outlet stream from the SR at 850 °C is mixed with compressed air also at 28 bar, which adds N_2 and O_2 to the process gas.

Secondary reforming (R-X12) is carried out and the effluent gas is cooled by heating the inlet to the SR. It is then sent to the next section. This effluent gas contains less than 0.3 vol% of CH_4, as seen in Table 12 and as expected from Aika et al. (1995).

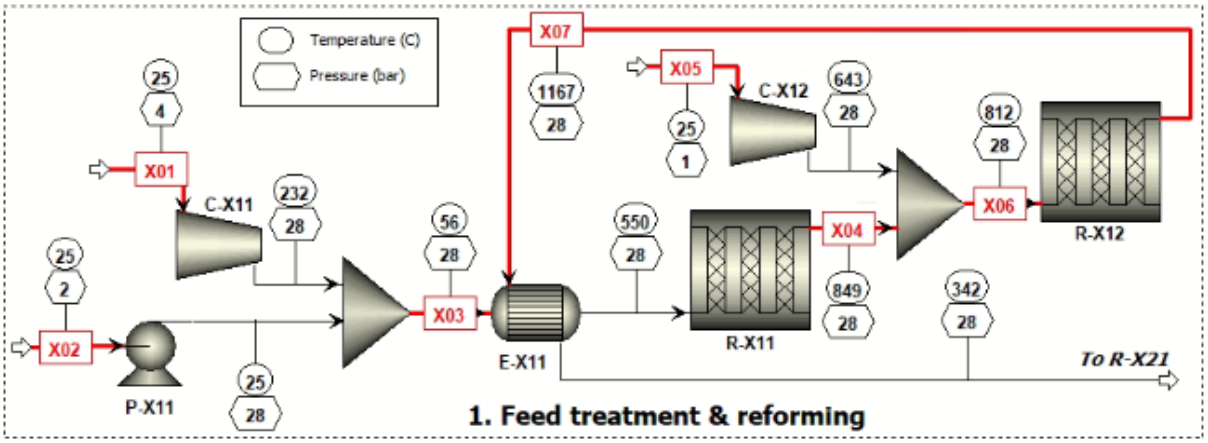

Figure 11 – First section of the conventional route.

Table 12 – Molar composition of the streams in the first section of the conventional route.

	X01	X02	X03	X04	X05	X06	X07
Mole flow (Mmol/h)	1.42	4.20	5.62	7.76	1.99	9.75	9.99
Composition (mole fraction)							
CH_4	1.00		0.25	0.04		0.03	1.39E-4
H_2O		1.00	0.75	0.35		0.28	0.32
CO_2				0.06		0.04	0.04
CO				0.08		0.07	0.10
H_2				0.47		0.37	0.38
N_2					0.78	0.16	0.16
Ar					0.01	2.04E-3	1.99E-3
O_2					0.21	0.04	

In the second section (Figure 12), the process gas rich in H_2 and CO undergoes two WGS processes: HTS (R-X21) and LTS (R-X22), respectively. Since the WGS reaction is exothermic, temperature rises are expected in the effluent gases of both reactors. The process gas is cooled to 200 °C between the two reactors. After LTS, the process gas stream has only traces of CO. The gas is cooled to 30 °C with CW and directed to a flash separator (V-X21) to remove excess water.

Molar compositions of CO must be around 3% at the HTS effluent gas and in the range from 0.1 to 0.3% after the LTS reactor (APPL, 2011). Table 13 shows that the streams follow the previous statement.

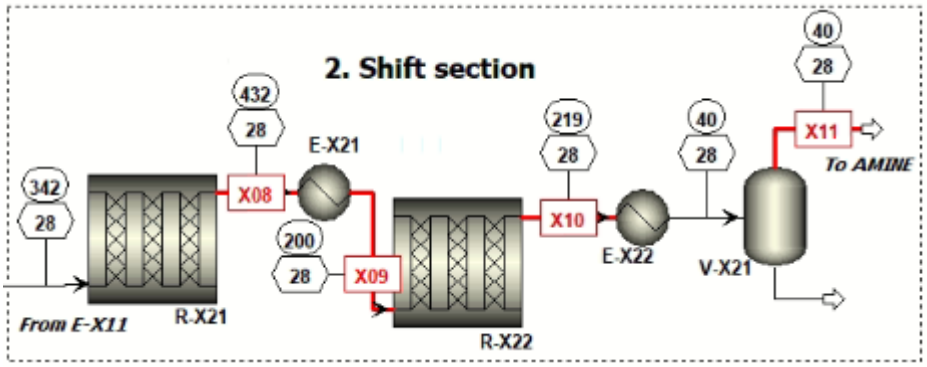

Figure 12 – Second section of the conventional route.

Table 13 – Molar composition of the streams in the second section of the conventional route.

	X08	**X09**	**X10**	**X11**
Mole flow (Mmol/h)	9.99	9.99	9.99	7.75
Composition (mole fraction)				
CH_4	1.39E-04	1.39E-04	1.39E-04	1.79E-04
H_2O	0.24	0.24	0.23	2.57E-03
CO_2	0.12	0.12	0.14	0.18
CO	0.02	0.02	3.53E-03	4.55E-03
H_2	0.46	0.46	0.48	0.61
N_2	0.16	0.16	0.16	0.20
Ar	1.99E-03	1.99E-03	1.99E-03	2.56E-03

The third section (Figure 13) is responsible for removing all CO_2 from the process gas, regenerating it in a separate stream (which is directed to urea synthesis), and to convert all traces of CO and CO_2 into CH_4, since the former are poisons to the ammonia catalyst and the latter is not.

Process gas from V-X21 is sent to the amine scrubbing process, which is represented in Figure 13 as a hierarchy named “AMINE”. The process gas exiting the amine scrubbing process has only traces of Ar, CH_4, CO, CO_2, and is rich in H_2 and N_2. This gas is then heated to 350 °C in a fired heater (H-X31) and methanation can occur next in R-X31. The effluent gas is sent to the last purification step.

Table 14 presents the details of the streams involved in this step. It is observed that stream X12 is in accordance to the expected values of 0.2 to 0.5% of CO and 0.005 to 0.02% of CO_2 (APPL, 2011).

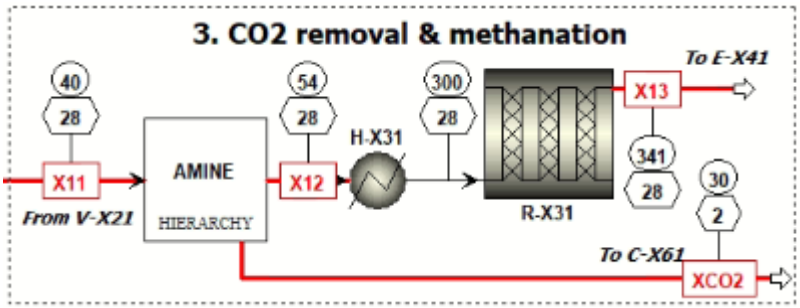

Figure 13 – Third section of the conventional route.

Table 14 – Molar composition of the streams in the third section of the conventional route.

	X11	**X12**	**X13**	**XCO_2**
Mole flow (Mmol/h)	7.75	6.33	6.26	1.43
Composition (mole fraction)				
CH_4	1.79E-04	2.17E-04	5.82E-03	9.39E-06
H_2O	2.57E-03	5.17E-03	0.01	0.02
CO_2	0.18	1.34E-05		0.94
CO	4.55E-03	5.52E-03		1.92E-04
H_2	0.61	0.74	0.73	0.03
N_2	0.20	0.24	0.25	6.28E-03
Ar	2.56E-03	3.10E-03	3.14E-03	1.43E-04

The fourth section, shown in Figure 14, starts with the process gas being cooled so that excess water can be removed in a flash separator (V-X41). A drying step takes place using 5A molecular sieves as adsorbent. Afterwards, the process gas is technically free of all oxygenated compounds (CO, CO_2, and H_2O) and is ready for compression to 200 bar in a four-stage compressor with intercooling (C-X41).

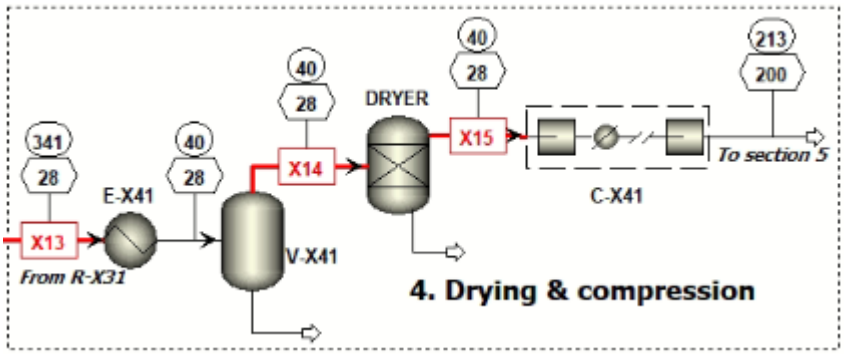

Figure 14 – Fourth section of the conventional route.

Table 15 presents the details of the streams in the fourth section. It is important to note that the process gas no longer has CO and CO_2 in its composition.

Table 15 – Molar composition of the streams in the fourth section of the conventional route.

	X13	**X14**	**X15**
Mole flow (Mmol/h)	7.75	6.21	6.19
	Composition (mole fraction)		
CH_4	5.82E-03	5.87E-03	5.88E-03
H_2O	0.01	2.45E-03	
H_2	0.73	0.74	0.74
N_2	0.25	0.25	0.25
Ar	3.14E-03	3.16E-03	3.17E-03

The fifth section is common to both configurations and features a hierarchy named “SYNTH”, corresponding to the ammonia quench reactor. The modeling of the reactor will be unfolded in a subsequent subsection. Figure 15 displays the details of the ammonia synthesis loop.

This section starts with the compressed process gas being mixed with recycled H_2 and N_2. This mixture is then directed to the quench reactor and cooled afterwards so that liquid NH_3 is directed to urea synthesis and the unreacted gases are recycled. A purge stream (X20) is needed to avoid inerts buildup (Ar and CH_4). The optimal purge percentage for the conventional route was found to be 1%. Streams details are shown in Table 16.

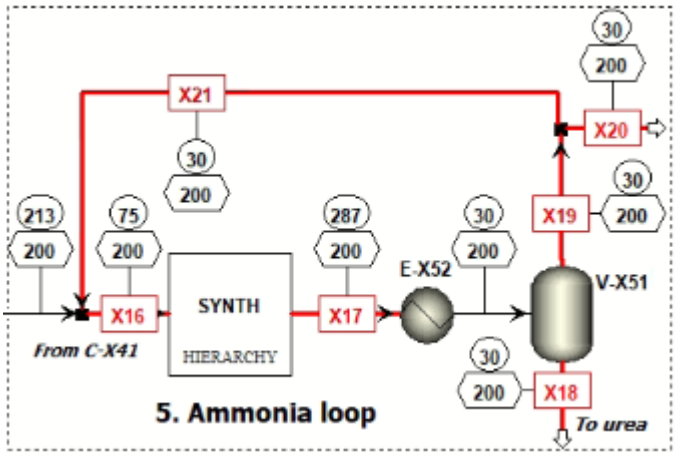

Figure 15 – Fifth section of the conventional route.

Table 16 – Molar composition of the streams in the fifth section of the conventional route.

	X16	X17	X18	X19	X20	X21
Mole flow (Mmol/h)	23.11	20.14	3.05	17.08	0.17	16.91
Composition (mole fraction)						
CH_4	0.04	0.04	9.18E-03	0.05	0.05	0.05
H_2	0.64	0.52	0.01	0.61	0.61	0.61
N_2	0.23	0.19	5.05E-03	0.22	0.22	0.22
Ar	0.02	0.02	5.28E-03	0.02	0.02	0.02
NH_3	0.08	0.24	0.97	0.11	0.11	0.11

The sixth and final section (Figure 16) is also common to both configurations, but with minor differences. They consist in reducing liquid NH_3 exiting the loop synthesis to 40 °C and 140 bar, and then reacting it with CO_2 compressed to 140 bar. The CO_2 stream comes from the amine scrubbing section, where pure CO_2 was regenerated from the process gas. The temperature target for CO_2 is between 250 and 300 °C, before entering the urea reactor. After compression in E-X62, CO_2 has a temperature of 578 °C, which is then used to generate HPS and cool it.

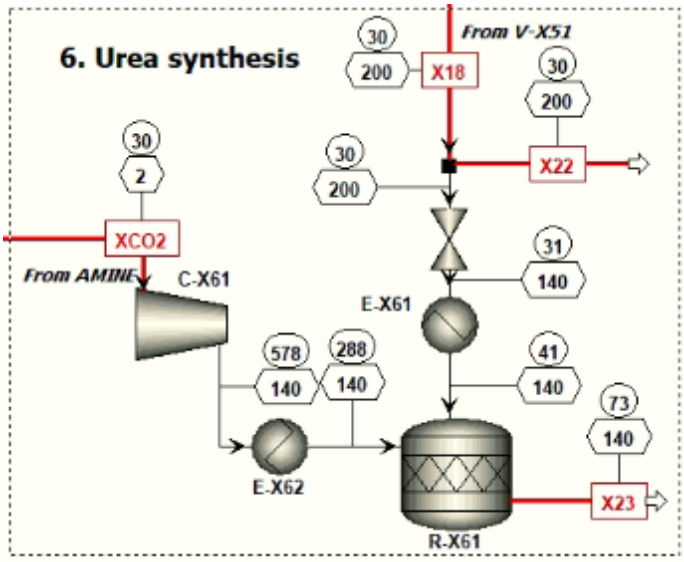

Figure 16 – Sixth section of the conventional route.

Table 17 presents the data from the sixth and final section of the conventional process. The product stream (X23) has a production of 1.33 Mmol/h of urea, which corresponds to an output of 1921.57 tonne/day.

Table 17 – Molar composition of the streams in the sixth section of the conventional route.

	XCO_2	**X18**	**X22**	**X23**
Mole flow (Mmol/h)	1.43	3.05	0.27	2.88
Composition (mole fraction)				
CH_4	9.39E-06	9.18E-03	9.18E-03	8.86E-3
H_2O	0.02			0.47
CO_2	0.94			4.67E-3
CO	1.92E-04			9.58E-05
H_2	0.03	0.01	0.01	0.03
N_2	6.28E-03	5.05E-03	5.05E-03	0.01
Ar	1.43E-04	5.28E-03	5.28E-03	0.01
NH_3		0.97		0.01
Urea				0.46

7.5.2. The innovative route

The process flow diagram for the innovative route is shown in Figure 17.

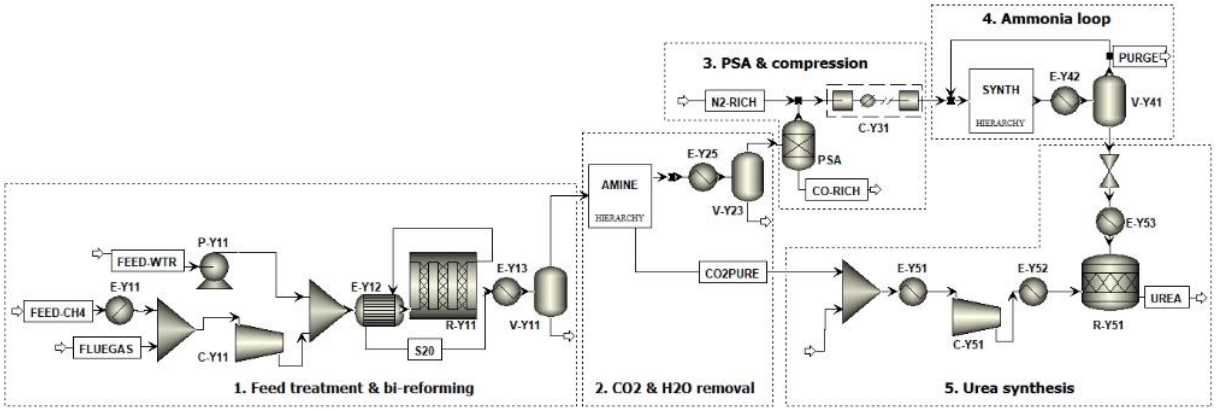

Figure 17 – Final PFD for the innovative route.

The first section, shown in detail in Figure 18, features the required feed treatment for the BRM process and the BRM reaction itself. Natural gas (Y02) is mixed with the flue gas (H_2O/CO_2 ratio of 2) from a power plant (Y01) and the mixture is compressed to 10 bar. Excess water (Y03) is also pumped to 10 bar and added to the mixture, so that a 3:3:1

ratio of CH_4:H_2O:CO_2 is reached. This mixture is heated to 550 °C in E-Y12, by using the BR outlet stream as hot stream, and feed the BR (R-Y11).

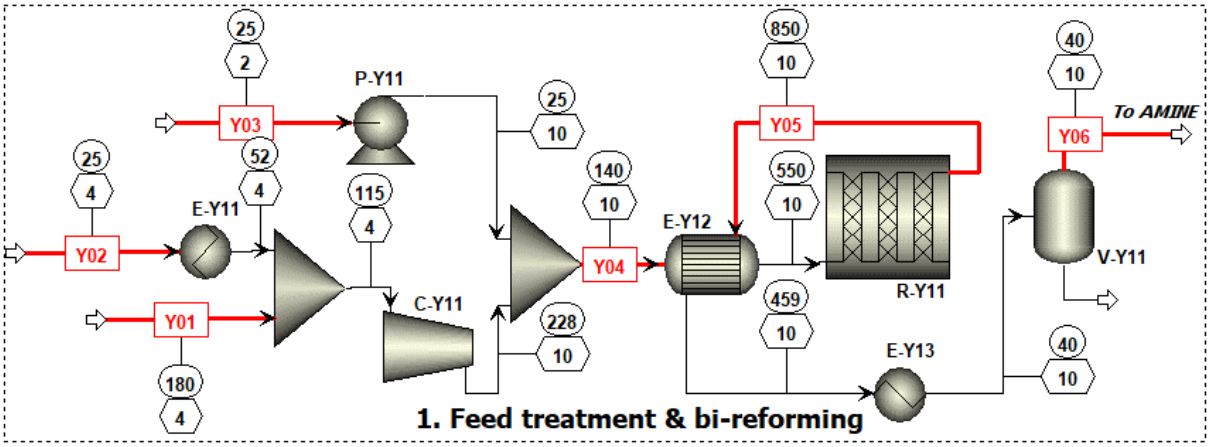

Figure 18 – First section of the innovative route.

The outlet stream from the BR at 850 °C is cooled to 40 °C and sent to a flash separator (V-Y11) so that excess steam can be removed. The streams featured in this section are shown in Table 18.

Table 18 – Molar composition of the streams in the first section of the innovative route.

	Y01	**Y02**	**Y03**	**Y04**	**Y05**	**Y06**
Mole flow (Mmol/h)	2.35	2.35	0.78	5.48	8.98	8.04
Composition (mole fraction)						
CH_4		1.00		0.43	0.07	0.07
H_2O	0.67		1.00	0.43	0.11	0.01
CO_2	0.33			0.14	0.04	0.05
CO					0.24	0.27
H_2					0.54	0.60

In the second section (Figure 19), process gas rich in H_2 and CO is sent to the same "AMINE" hierarchy as the conventional process, where CO_2 is removed and regenerated in a separate stream.

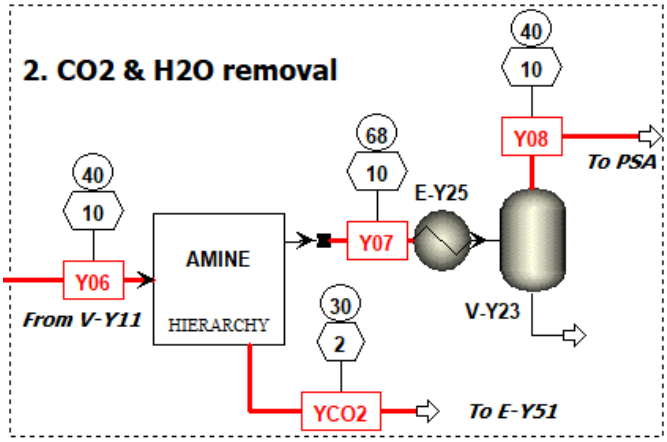

Figure 19 – Second section of the innovative route.

After CO_2 removal, process gas is sent to the last purification step, so that high-purity H_2 can be obtained. Unlike the conventional route, the innovative route only has two major purification processes (amine scrubbing and PSA). Streams from the second section are detailed in Table 19.

Table 19 – Molar composition of the streams in the second section of the innovative route.

	Y06	**Y07**	**Y08**	**YCO_2**
Mole flow (Mmol/h)	8.04	7.79	7.64	7.75
Composition (mole fraction)				
CH_4	0.07	0.08	0.08	1.43E-3
H_2O	0.01	0.03	0.01	0.02
CO_2	0.05	0.00	0.00	0.96
CO	0.27	0.27	0.28	3.95E-3
H_2	0.60	0.62	0.63	0.01

In the third section (Figure 20), process gas is sent to a PSA process, where high-purity (99.999%) H_2 is obtained, with 86 mol% recovery (GUOXUE et al., 2013). The outlet stream of the PSA process is a CO-rich stream, which can be sold as fuel or for Fischer-Tropsch processes. For this work, this stream will be sold as a fuel stream.

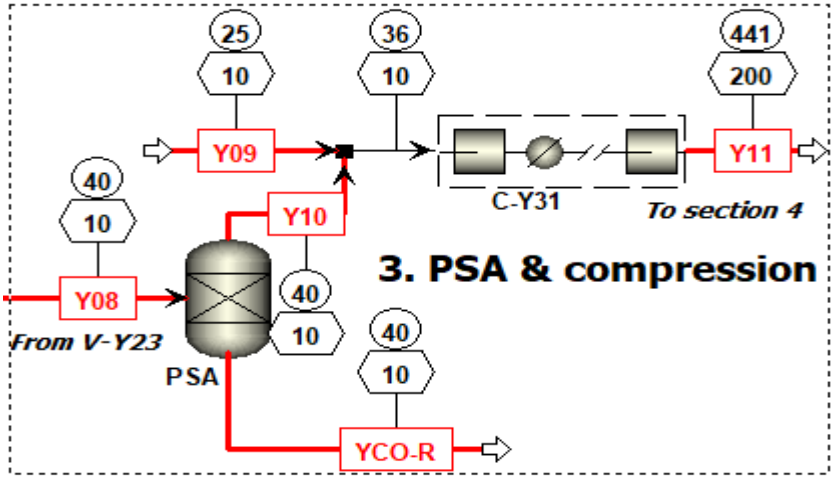

Figure 20 – Third section of the innovative route.

External N_2 (Y09) is mixed with high-purity H_2 from the PSA section (Y10). The amount of inlet N_2 is just enough to achieve the desired 1:3 ratio of N_2:H_2. Unlike the conventional process, the innovative route does not require a methanation step or any other process to specifically remove traces of CO, CO_2, and H_2O, since all of these are removed in the PSA process. This reduces the number of required equipment in the innovative route.

Once ready for ammonia synthesis, the gas is compressed in a 4-stage compressor with intercooling (C-Y31), and then sent to the ammonia section. Table 20 presents the breakdown of the featured streams in this section.

Table 20 – Molar composition of the streams in the third section of the innovative route.

	Y08	**Y09**	**Y10**	**Y11**	**YCO-R**
Mole flow (Mmol/h)	7.64	1.39	4.17	5.56	3.47
Composition (mole fraction)					
CH_4	0.08				0.17
H_2O	0.01				0.01
CO_2	0.00				
CO	0.28				0.62
H_2	0.63		1.00	0.75	0.20
N_2		0.99		0.25	
Ar		1.00E-4			

The fourth section, shown in Figure 21, is the same as the fifth section of the conventional route. Ammonia synthesis and separation, as well as H_2 and N_2 recycling, are carried out in the same way as the conventional process. The main differences are the inlet and outlet streams of the reactor and the purge ratio, whose optimal value was 0.0022% due to the extremely low content of inerts (traces of Ar), as opposed to the conventional route that has traces of Ar and CH_4.

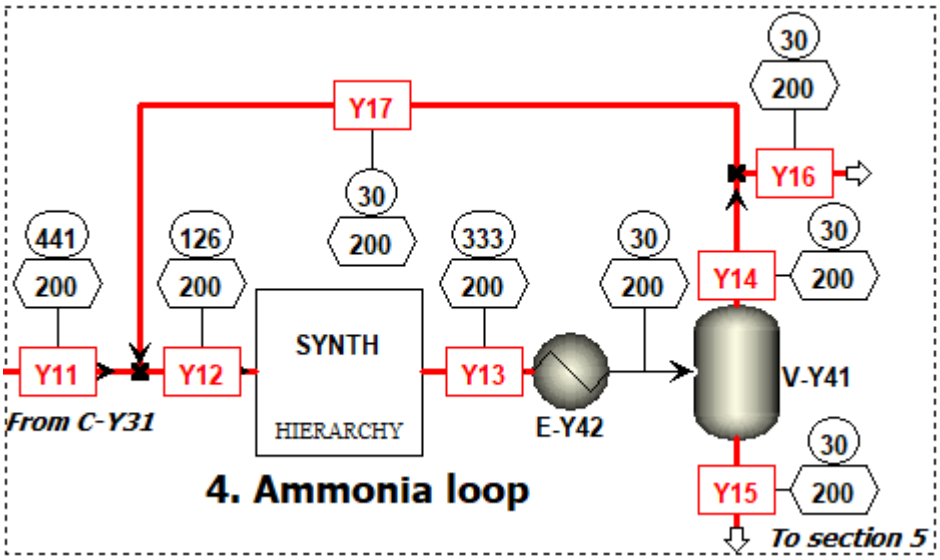

Figure 21 – Fourth section of the innovative route.

The streams in this section are depicted in Table 21, with Ar removal due to its extremely low content.

Table 21 – Molar composition of the streams in the fourth section of the innovative route.

	Y11	**Y12**	**Y13**	**Y14**	**Y15**	**Y16**	**Y17**
Mole flow (Mmol/h)	5.56	22.43	19.69	16.91	2.78	0.04	16.87
Composition (mole fraction)							
H_2	0.75	0.69	0.58	0.68	0.01	0.68	0.68
N_2	0.25	0.23	0.19	0.23	0.00	0.23	0.23
NH_3		0.07	0.22	0.10	0.98	0.10	0.10

The fifth and last section, shown in Figure 22, is almost the same as the last section of the conventional route. The main differences are: the conventional route does not produce excess NH_3, but it uses external CO_2 (from flue gas) so that all produced NH_3 can be

converted to urea. External CO_2 (Y18) is mixed with pure CO_2 from the amine scrubbing section (YCO_2), and the mixed stream is cooled to 30 °C and compressed to 140 bar. It generates HPS in E-Y52 and it is reacted with cooled NH_3 from the previous section.

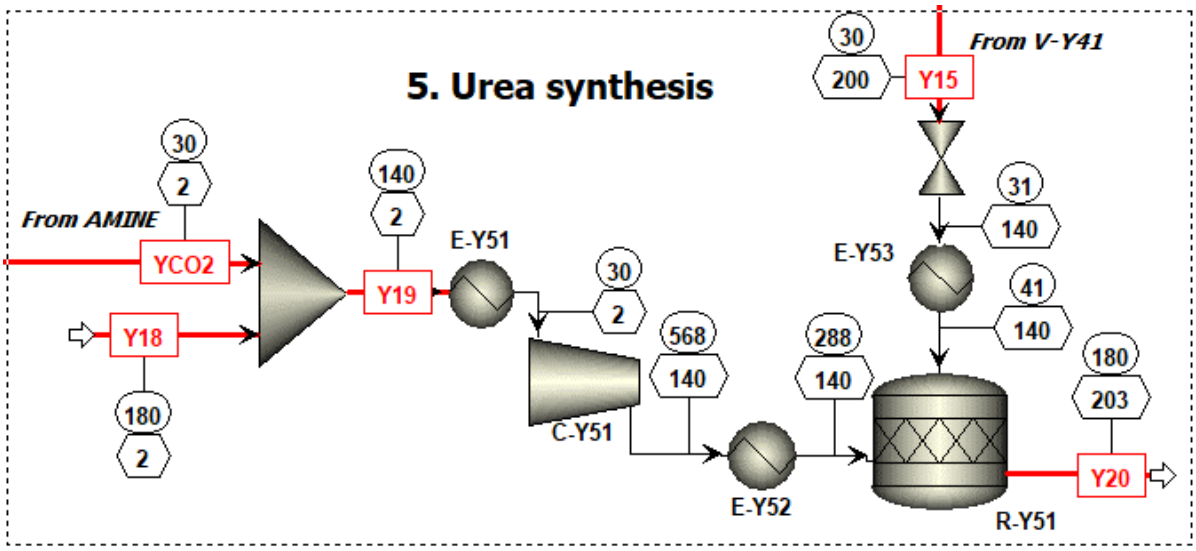

Figure 22 – Fifth section of the innovative route.

Table 22 presents the data from the streams of the final section. The product stream (Y20) has a production of 1.35 Mmol/h of urea, which corresponds to an output of 1952.07 tonne/day.

Table 22 – Molar composition of the streams in the fifth section of the innovative route.

	YCO_2	**Y15**	**Y18**	**Y19**	**Y20**
Mole flow (Mmol/h)	0.39	2.78	0.99	1.38	2.81
Composition (mole fraction)					
H_2O	0.02			0.01	0.49
CO_2	0.96		1.00	0.99	
H_2	0.01	0.01			0.01
N_2		4.86E-3			
NH_3		0.98			0.01
Urea					0.48

7.5.3. The ammonia quench reactor

The configuration of the ammonia quench reactor was taken from Araújo and Skogestad (2008). As seen in Figure 23, the reactor features 3 beds with quench flows between them. The inlet process gas is separated in varying percentages in separators S1, S2, and S3 to cool the synthesis gas coming out of the beds, as seen in Table 23.

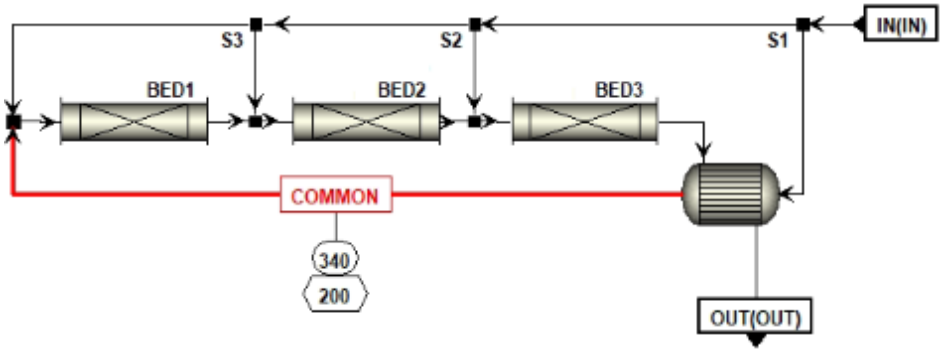

Figure 23 – Layout of the ammonia quench reactor for both configurations.

Table 23 – Split fraction of the separator inlet stream directed to quenching.

	To Bed 1	**To Bed 2**	**To Bed 3**
Split fraction	0.500	0.256	0.377

Since there are slight differences between the mole fractions and operating temperatures for both processes, the details of the streams for each route will not be presented in detail. The only similarity between both routes is that the "COMMON" stream in red in Figure 23 has the same operating temperature and pressure, as shown.

Although the inlets and outlets of each process vary, their global conversion (based on H_2) and temperatures are nearly the same, as seen in Table 24. Global conversions were calculated considering the molar flow of H_2 entering the first bed and the molar flow of H_2 exiting the last bed.

Table 24 – H_2 conversion and operating temperatures of each reactor bed for both routes.

		Bed 1		**Bed 2**		**Bed 3**	
		T_{in} (°C)	**T_{out} (°C)**	**T_{in} (°C)**	**T_{out} (°C)**	**T_{in} (°C)**	**T_{out} (°C)**
Conventional	**Temperature (°C)**	256.1	438.9	379.5	429.7	383.3	423.6
	Conversion (%)	25.5		8.7		7.2	
	Global conversion (%)				30.0		
Innovative	**Temperature (°C)**	272.1	455.9	401.7	448.5	406.2	443.6
	Conversion (%)	23.0		7.1		5.8	
	Global conversion (%)				26.4		

The values of global conversions and operating temperatures are in accordance to the data widely reported in the literature, which state that global conversions range from 20 to 32% and operating temperatures should be kept between 300 and 500 °C (AIKA et al., 1995; ELNASHAIE; ELSHISHINI, 1993; TAVARES; MONTEIRO; MAINIER, 2013).

The innovative route, however, has a slightly lower value of global conversion, due to its slightly higher process gas temperatures before each bed. The reason for that is the minor differences between temperatures of the process gas exiting the 4-stage compressor and their small differences in gas composition. Since the ammonia synthesis reaction is exothermic (Eq. 8), higher temperatures result in lower conversions.

7.6. UTILITIES COSTS AND CO_2 EMISSION RATES

Since both configurations have different equipment, their utilities usage is different, and, as expected, their CO_2 emissions are also different. In this section, utilities usage, costs, and CO_2 emissions for all equipment are presented.

The detailed data for each equipment for both routes can be found in Appendix A. Heat exchangers not shown in Tables A1 and A2 are process heat exchangers, and therefore no utilities are required.

From Tables A1 and A2, it can be seen that both routes have similar CO_2 emissions and similar utilities costs, despite the conventional route having more equipment

requirements. The innovative route, however, use CO_2 as raw material, which affects the total CO_2 mass balance, either for lower emissions or even negative emissions (abatement).

7.7. RAW MATERIALS AND PRODUCTS

In this section, a breakdown of raw materials usage and product generation is presented.

Table 25 presents the mass flows of products and raw materials for each configuration.

Table 25 – Breakdown of products and raw materials for each configuration.

	Products (tonne/h)			**Raw materials (tonne/h)**					
	Urea	**NH_3**	**CO-rich stream**	**NG[1]**	**NG[2]**	**Water[1]**	**Air**	**CO_2**	**N_2**
Conventional	80.01	4.47	–	22.46	7.14	75.66	57.52	–	-
Innovative	81.34	–	71.85	37.68	10.00	42.31	-	78.01	38.99

(1): as an inlet to both reformers;
(2): in utilities.

Table 25 shows that both configurations have nearly the same urea production, and it is close to the nominal target of 2000 MTPD, as stated in Chapter 5. As expected, the conventional route produces excess NH_3, since its limiting reactant for urea production is CO_2.

As for NG consumption as raw material, the innovative route consumes more NG, due to the stoichiometry of the reforming reactions (the innovative route produces 2.67 moles of H_2 per mole of CH_4, while the conventional route produces 3.00 and the additional H_2 generated in the WGS sections).

Consumption of NG in utilities is also higher in the innovative route, mainly due to the heat duty needed to operate the BR as opposed to the SR (500.53 GJ/h and 311.63 GJ/h, respectively, as shown in Appendix A).

Water consumption is higher in the conventional route, since it does not have any other form of obtaining the required amount of water, unlike the flue gas of the innovative route, which already contains steam.

Detailed discussions on CO_2 will be covered in Section 7.10.

As previously mentioned in subsection 7.5.2, the CO-rich stream from the innovative process is sold as fuel to other processes. The net heating value (NHV) parameter was chosen to be the basis of the price definition for the stream, whose price will be proportional to the NHV of CH_4 (50.00 GJ/tonne, taken from Aspen Plus).

Table 26 shows the composition of the CO-rich stream, as well as its calculated NHV from Aspen Plus.

Table 26 – Composition and net heating value of the CO-rich stream.

	Mole flow (Mmol/h)	**Mass flow (tonne/h)**
Total	3.47	71.85
	Mole fractions	**Mass fractions**
CH_4	0.17	0.13
H_2O	0.01	0.01
CO_2	3.64E-05	7.74E-05
CO	0.62	0.83
H_2	0.20	0.02
	NHV (GJ/tonne)	17.42

Using data from Table 3 and Table 25, a thorough analysis was carried on both routes, and the results are shown in Table 27 for the conventional route and Table 28 for the innovative route.

Table 27 – Revenues and expenses for the conventional route.

	Cost ($/year)
Natural Gas (as RM)*	-38,481,955
Water	-1,058,874
Air	-27,091,872
Ammonia	+9,307,366
Urea	+163,981,681

(*): NG usage as utilities is already considered under utilities usage.

Table 28 – Revenues and expenses for the innovative route.

	Cost ($/year)
Natural Gas (as RM)*	-63,657,724
Water	-518,769
External N_2	-24,685,881
CO_2 (as RM)	+38,986,906
CO-rich stream	+42,238,219
Urea	+166,510,664

(*): NG usage as utilities is already considered under utilities usage.

7.8. ECONOMIC METRICS AND ANALYSIS

Although the previous section describes in detail the revenues and expenses for both configurations, other relevant data for the full economic analysis is missing, such as labor costs, equipment costs, and the fixed capital investment.

7.8.1. Equipment costs breakdown

Detailed equipment costs for both configurations can be found in Appendix B. Tables B1 and B2 detail costs for the conventional and innovative routes, respectively. As mentioned before, equipment pricing was performed following the methodology described in Turton et al. (2008) and the premises in Section 6.6. A general overview of how much each type of equipment affects the final cost can be seen in Figure 24 and Figure 25.

As seen in the Figures 24 and 25, compressors and drives account for nearly 30% of the final costs for both routes. Although the innovative route operates at lower pressure than the conventional route, it still needs high investments in compressors. As for reactors, the innovative route has only the ammonia reactor, which is the same in the conventional route. Still, the impact of the other reactors in the conventional route (LTS, HTS, and methanator) is small.

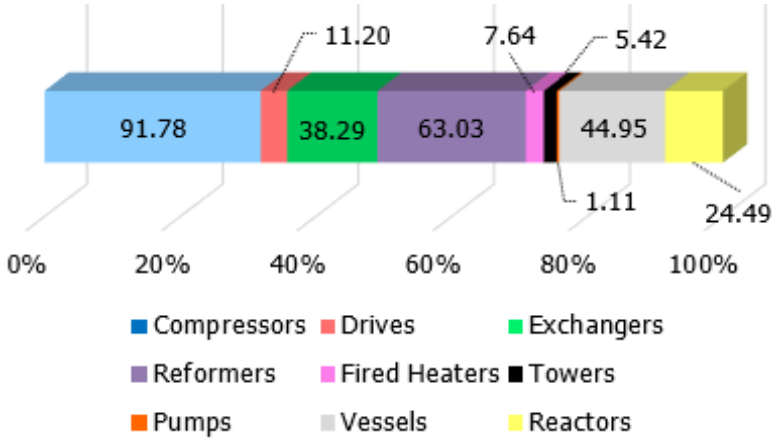

Figure 24 – Breakdown of equipment costs for the conventional route (in MM$).

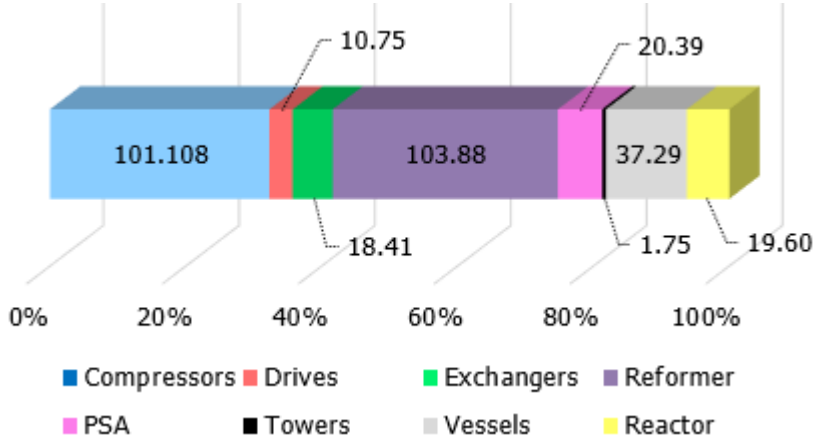

Figure 25 – Breakdown of equipment costs for the innovative route (in MM$).

For the reformers, the bi-reformer is more expensive than both reformers in the conventional route, probably because of its higher requirement of volume and heat to generate enough H_2 to be comparable to the same amount generated in the conventional route. The bi-reformer also demands a higher flow of raw materials than the steam reformer.

Heat exchangers in the conventional route are almost double the price than in the innovative route. This is mainly due to the many temperature adjustments required in the conventional route, especially cooling of the process gas either after or before reactors.

Flash separator (vessels) costs are nearly the same for both configurations, since both have the same number of vessels (4). The flash separator in the ammonia synthesis loop accounts for almost 98% of the total cost of vessels, due to its high operation pressure, which heavily impacts capital costs.

Towers and pumps have nearly the same impact in both routes, with pump costs being so negligible in the innovative route that it was not shown in Figure 25 (less than 0.01%).

7.8.2. Cash flow analysis

Cash flow analysis is another important economic data in economic analysis of processes. Herein the methodology from Turton et al. (2008) was considered and its details can be found in Appendix C.

Results from the cash flow analysis, discounted cash flows and discounted cumulative cash flows, for both routes are shown in Figure 26. The cumulative cash flow in the last year represents the chosen economic metric to be evaluated: the net present value.

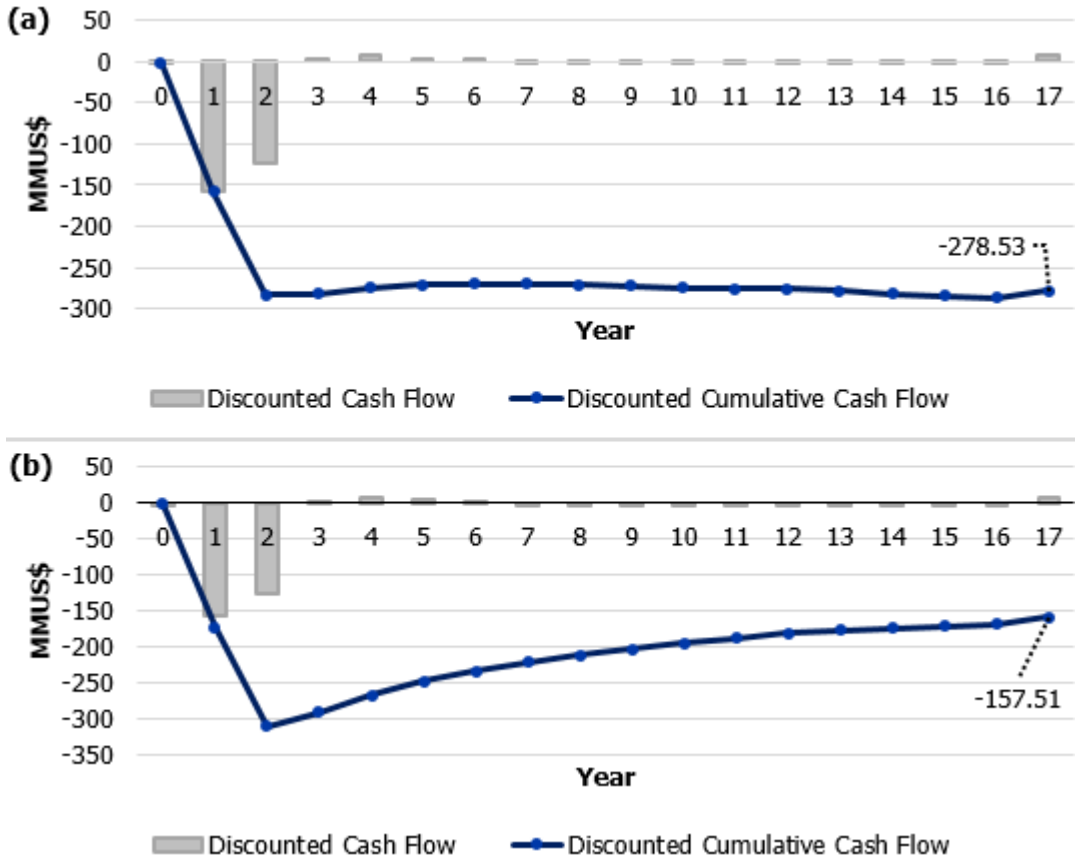

Figure 26 – Discounted cash flow analysis and NPV for: (a) the conventional route; (b) the innovative route.

Figure 26 shows that both configurations are not economically feasible. Investing in any of both configurations would lead to capital losses. Interestingly, the innovative route has a higher NPV than its counterpart, despite the higher requirement of capital and operating costs, mainly due to the revenue from the CO-rich stream.

Another factor that impacts the economic outcome of both routes is the process optimization. Both routes were not optimally designed, due to the enormous amount of time and work that would be required for such a thing. The goal of this work was to create a conceptual design for both configurations, only for initial analyses, and to compare a century-long existing process with an innovative one with high potential for CO_2 abatement.

7.8.3. Economic sensitivity analysis

Sensitivity analysis was performed in different economic scenarios (i.e. different prices for raw materials and products) and compared to the base case. In the first analysis (hereafter called "analysis A"), scenarios where the NPV for the innovative route would be zero were evaluated, first by changing NG prices (case #A1) and then changing urea prices (case #A2). Prices of CO_2 were also changed (case #A3). The results are shown in Table 29.

Table 29 – Results of Analysis A for both configurations.

		Base case	**Case #A1**	**Case #A2**	**Case #A3**
	Prices ($/tonne)	**NG: 202.90** **Urea: 246.00** **NH_3: 250.00** **CO_2: 60.00**	**NG: 55.26** **Urea*: 246.00** **NH_3: 250.00** **CO_2: 60.00**	**NG: 202.90** **Urea*: 308.56** **CO_2: 60.00**	**NG: 202.90** **Urea: 246.00** **NH_3: 250.00** **CO_2: 125.50**
NPV (MM$)	**Conventional**	-278.53	-105.82	-109.85	-278.53
	Innovative	-157.51	0.00	0.00	0.00

(*): Ammonia prices were considered to be the same as urea prices.

In the second analysis (hereafter called "analysis B"), average yearly prices from 2017 (case #B1) and 2018 (case #B2) were used to evaluate revenues and expenses, as featured in Table 30. It is important to note that the base case features the yearly average prices from 2019.

Table 30 – Results of Analysis B for both configurations.

		Case #B1	Case #B2	Base case
	Prices ($/tonne)	**NG: 211.70 Urea: 225.00 Ammonia: 283.00 CO_2: 60.00**	**NG: 218.5 Urea: 261.00 Ammonia: 315.00 CO_2: 60.00**	**NG: 202.90 Urea: 246.00 Ammonia: 250.00 CO_2: 60.00**
NPV (MM$)	**Conventional**	-328.27	-243.52	-278.53
	Innovative	-215.43	-133.65	-157.51

As seen in Table 29 and Table 30, both configurations are not economically feasible in many different scenarios. As mentioned before, design and process optimizations could reduce utilities usage and equipment costs, which, in turn, could make these routes profitable.

Natural gas is the basis of both routes, and their profitability depends on low natural gas prices. Since the early 2000s, prices have been fluctuating up and down, which makes the profitability of ammonia and urea plants very unpredictable. It is impossible to establish a "worldwide natural gas price", since its price depends on many factors, especially regional availability and production. As an example, France and Italy are huge consumers of Russian natural gas, which reaches these countries via a pipeline across Ukraine. Tensions between Russia and Ukraine have led to natural gas shutoffs, making prices skyrocket in these countries (UNION OF CONCERNED SCIENTISTS, 2015).

In Brazil, ammonia and urea production is technically impracticable. Firstly because of high levels of CO_2 in Brazilian natural gas and, secondly, because of the lack of infrastructure for natural gas transportation and processing. All these factors make natural gas prices in Brazil quite expensive. As a matter of comparison, in May 2020, Russia's natural gas for industrial uses in Europe was sold for $1.58/MMBtu, while the prices in the Henry Hub (USA) were around $1.75/MMBtu. Brazil's price was around $10.80/MMBtu (EPBR, 2020).

In 2018, the worldwide urea market was evaluated at around $12.9b. Unsurprisingly, the top-3 exporters were countries where natural gas is cheap. Russia comes first with a 12.50% market share, followed by Qatar at 9.69% and Saudi Arabia at 9.31%. On the other hand, Brazil is the top importer, with an 11.80% share (corresponding to $1.3b), followed by the US at 11.50% and India at 11.30%. The top-3 countries that export urea to

Brazil are Russia, with 24.30% of total imports, followed by Algeria at 16.80% and Qatar at 11.10% (OEC, 2020).

Finally, natural gas is the key player in ammonia and urea production. Countries where natural gas is expensive, such as Brazil, would hardly achieve profitability if either production routes (conventional or innovative) were to be invested on. Not surprisingly, Brazil had the operation of two urea plants based on natural gas discontinued and, in 2017, one of them had a deficit of R$ 200 million and the other one a deficit of R$ 600 million (SINDIPETRO BA, 2020).

7.9. TECHNICAL METRICS

Technical metrics for both configurations are shown in Figure 27. As described in Section 6.7, these metrics relate how well the inputs (mass of raw materials, electric energy, and thermal energy) are being used in each process to generate its products. As a reminder: lower values represent higher performances.

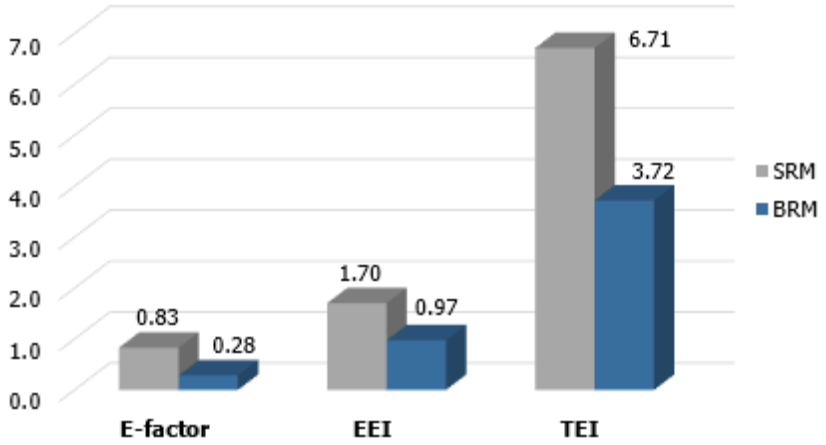

Figure 27 – Technical metrics for both configurations.

As seen in Figure 27, the innovative route has the best performance for all metrics. Its better performance in raw materials usage (E-factor) is due to its CO-rich stream. Since both routes produce the same amounts of urea, the innovative route has the upper hand in that it also produces a CO-rich stream with nearly the same mass flow of urea. The conventional route has a 155.64 tonne/h mass flow of inputs, while the innovative route has a slightly higher mass input of 196.63 tonne/h. The mass flow of outputs, however, is almost

double for the innovative route (85.01 tonne/h for the conventional route and 153.18 tonne/h for the innovative route), which means a better usage of raw materials.

The electric energy performance (represented in EEI) is also better for the innovative route due to its higher mass flow of outputs, since both configurations have nearly the same electric energy usage (40.22 MWh/tonne of products for the conventional route and 41.44 MWh/tonne of products for the innovative route).

The thermal energy performance (represented in TEI) follows the same reasoning as EEI. The conventional route has a thermal energy usage of 570.77 GJ/h while the innovative route has a usage of 570.28 GJ/h. However, once again, the higher mass flow of outputs of the innovative route is responsible for driving the indicator down.

All these referred values of inputs and outputs used in Figure 27 can be found in Table 25 and Appendix A.

7.10. ENVIRONMENTAL METRICS

Environmental metrics for both configurations are shown in Figure 28. As described in Section 6.8, these metrics relate how much CO_2 is associated with inputs usage (mass of CO_2 as raw material and CO_2 emissions from electric energy and thermal energy generation) to the products generated by each route. Negative values represent a higher inlet flow of CO_2 when compared to its outlet flow (i.e. CO_2 abatement). As a reminder: lower values represent greener processes.

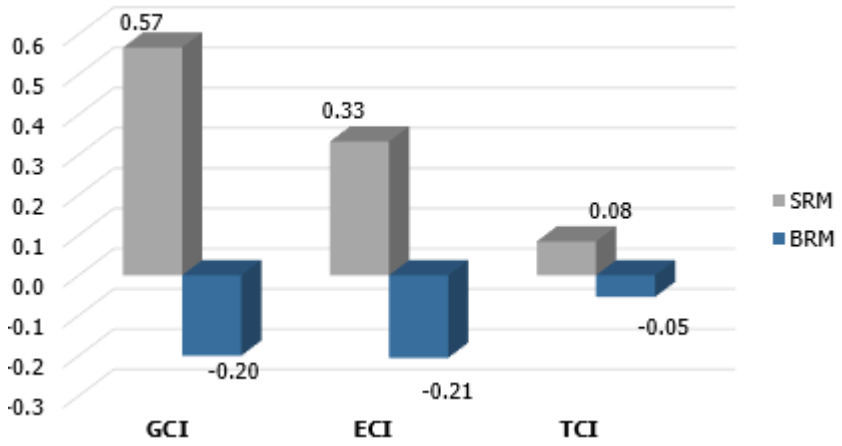

Figure 28 – Environmental metrics for both configurations.

The innovative route has negative values for all metrics, which means that the inlet of CO_2 to the process is higher than the outlet of CO_2. This ultimately shows that the innovative route indeed promotes CO_2 abatement. The innovative route has an inlet mass flow of 77.66 tonne/h of CO_2 (as RM), and an output of 47.00 tonne/h (from utilities, emissions in the ammonia synthesis loop purge stream, and emissions in the urea reactor), netting a total of -30.64 tonne/h of CO_2). The conventional route, however, has no inlet mass flow of CO_2, only an outlet of 48.18 tonne/h.

All these referred values of inputs and outputs used in Figure 28 can be found in Table 25 and Appendix A.

8. CONCLUSIONS

The proposed innovative route for ammonia and urea production has the potential to promote CO_2 abatement. This route is based on the bi-reforming of methane (BRM), which generates a higher mass flow output of products, but also consumes more thermal energy in its reforming reactor than the conventional route based on the steam reforming of methane (SRM). The BRM process also requires a higher reforming reactor volume than its counterpart.

Even though the conventional route operates on lower pressures and with less equipment, it has higher CAPEX and OPEX values than the conventional route. Both routes, however, are able to reach the nominal production target of 2000 MTPD.

From an economic point of view, both the innovative route and the conventional route are not profitable, although the former has better economic indicators (NPV). This is due to the high volatility of natural gas prices and low prices of urea and ammonia. If the investment were to be placed in a region with cheap natural gas prices, these processes might become profitable. Even though being not economically feasible, the innovative route is more prone to economic success than its counterpart. However, a detailed and optimal process design could also help with the profitability analysis of both routes.

Environmentally, the innovative route achieves a negative value of CO_2 emissions, meaning that it consumes rather than emits CO_2. Its counterpart, however, only emits CO_2. Emissions from both routes take into account all CO_2 emissions related to thermal energy and electric energy generation, as well as CO_2 from fired heaters (mainly the reformers) and CO_2 emissions from ammonia synthesis purge stream and unreacted CO_2 in the urea reactor. Negative emissions of CO_2 in chemical processes are an unusual feature.

Although being a greener and promising process, the BRM process is still in technological development. More research is needed on catalysts stability, performance and coke resistance in order to the BRM process may achieve commercial use.

8.1. SUGGESTIONS FOR FUTURE WORKS

- Development of a thorough kinetic model for the BRM process;
- Optimization of the innovative route, so that raw materials and utilities are used more efficiently, and equipment costs are reduced. This could also improve technical, economic and environmental metrics;
- Evaluate the feasibility of employing air distillation in the innovative route, so that no external N_2 is needed and the generated O_2 can be sent to the power plant. This would increase the integration between the innovative route and the power plant;
- Evaluate the feasibility of the integration of the innovative route and a conventional power plant (operated on NG and air). This could increase the number of scenarios where the innovative route could be employed, but could also increase equipment and feed treatment costs, since CO_2 capture with amines would be required;
- Analysis of other possible destinations of the CO-rich stream, such as butanol production or Fischer-Tropsch processes. Different destinations of this stream could improve economic metrics of the innovative route.

9. REFERENCES

AASBERG-PETERSEN, K.; BAK HANSEN, J. H.; CHRISTENSEN, T. S.; DYBKJAER, I.; CHRISTENSEN, P. S.; STUB NIELSEN, C.; WINTER MADSEN, S. E. L.; ROSTRUP-NIELSEN, J. R. **Technologies for large-scale gas conversion**. Applied Catalysis A: General, v. 221, n. 1–2, p. 379–387, Nov. 2001.

AIKA, K.; CHRISTIANSEN, L.; DYBKJAER, I.; HANSEN, B.; NIELSEN, P. E. H.; NIELSEN, A.; STOLTZE, P.; TAMARU, K. **Ammonia: catalysis and manufacture**. 1st. ed. Springer-Verlag, 1995.

ALBERTON, A. L.; SCHWAAB, M.; FONTES, C. E.; BITTENCOURT, R. C.; PINTO, J. C. **Hybrid modeling of methane reformers. 1. A metamodel for the effectiveness factor of a catalyst pellet with complex geometry**. Industrial and Engineering Chemistry Research, v. 48, n. 21, p. 9369–9375, 2009.

APPL, M. **Chemical Reactions and Uses of Ammonia**. In: Ammonia: Principles and Industrial Practice. Weinheim, Germany: Wiley-VCH Verlag GmbH, 2007a. p. 231–234.

APPL, M. **Process Steps of Ammonia Production**. In: Ammonia: Principles and Industrial Practice. Weinheim, Germany: Wiley-VCH Verlag GmbH, 2007b. p. 65–176.

APPL, M. **Ammonia, 2. Production Processes**. In: Ullmann's Encyclopedia of Industrial Chemistry. Weinheim, Germany: Wiley-VCH Verlag GmbH & Co. KGaA, 2011. v. 3p. 139–225.

APPL, M. **Ammonia, 3. Production Plants**. In: Ullmann's Encyclopedia of Industrial Chemistry. p. 227–261.

ARAÚJO, A.; SKOGESTAD, S. **Control structure design for the ammonia synthesis process**. Computers & Chemical Engineering, v. 32, n. 12, p. 2920–2932, Dec. 2008.

ARAÚJO, O. Q. F.; MEDEIROS, J. L.; YOKOYAMA, L.; MORGADO, C. R. V. **Metrics for sustainability analysis of post-combustion abatement of CO2 emissions: Microalgae mediated routes and CCS (carbon capture and storage)**. Energy, v. 92, p. 556–568, 1 Dec. 2015.

ASHIK, U. P. M.; VISWAN, A.; KUDO, S.; HAYASHI, J. **Nanomaterials as Catalysts**. In: Applications of Nanomaterials. Elsevier, 2018. p. 45–82.

AZEEM, B.; KUSHAARI, K.; MAN, Z. B.; BASIT, A.; THANH, T. H. **Review on materials & methods to produce controlled release coated urea fertilizer**. Journal of

Controlled Release, v. 181, n. 1, p. 11–21, 2014.

BARTHOLOMEW, C. H.; FARRAUTO, R. J. **Fundamentals of industrial catalytic processes**. 2nd. ed. John Wiley & Sons, 2006. v. 7

BUSTAMANTE, F.; ENICK, R. M.; CUGINI, A. V.; KILLMEYER, R. P.; HOWARD, B. H.; ROTHENBERGER, K. S.; CIOCCO, M. V.; MORREALE, B. D.; CHATTOPADHYAY, S.; SHI, S. **High-Temperature Kinetics of the Homogeneous Reverse Water-Gas Shift Reaction**. AIChE Journal, v. 50, n. 5, p. 1028–1041, 1 May 2004.

CARLSSON, M. **Carbon Formation in Steam Reforming and Effect of Potassium Promotion**. Johnson Matthey Technology Review, v. 59, n. 4, p. 313–318, 2015.

CHIBANE, L.; DJELLOULI, B. **Methane Steam Reforming Reaction Behaviour in a Packed Bed Membrane Reactor**. International Journal of Chemical Engineering and Applications, v. 2, n. 3, p. 147–156, 2011.

CHIYODA CORPORATION. **CO2 Reforming Process**. Available in: <https://www.chiyodacorp.com/en/service/gtl/co2-reforming/>. Accessed in: 21 Jul. 2019.

CPLC. **Report of the High-Level Commission on Carbon Prices**. Available in: <www.carbonpricingleadership.org>. Accessed in: 20 Sep. 2020.

DE DEKEN, J. C.; DEVOS, E. F.; FROMENT, G. F. **Steam Reforming of Natural Gas: Intrinsic Kinetics, Diffusional Influences, and Reactor Design**. In: p. 181–197.

DE GROOTE, A. M.; FROMENT, G. F. **Simulation of the catalytic partial oxidation of methane to synthesis gas**. Applied Catalysis A: General, v. 138, n. 2, p. 245–264, May 1996.

EDRISI, A.; MANSOORI, Z.; DABIR, B. **Urea synthesis using chemical looping process - Techno-economic evaluation of a novel plant configuration for a green production**. International Journal of Greenhouse Gas Control, v. 44, p. 42–51, 2016.

EDWARDS, R. W. J.; CELIA, M. A. **Infrastructure to enable deployment of carbon capture, utilization, and storage in the United States**. Proceedings of the National Academy of Sciences of the United States of America, v. 115, n. 38, p. E8815–E8824, 2018.

EIA. **U.S. Natural Gas Prices**. Available in: <https://www.eia.gov/dnav/ng/ng_pri_sum_dcu_nus_a.htm>. Accessed in: 20 Sep. 2020.

ELNASHAIE, S. S. E. H.; ELSHISHINI, S. S. **Modelling, Simulation and Optimization of Industrial Fixed Bed Catalytic Reactors**. Gordon & Breach Science Publishers, 1993. v. 7

EPA. **Environmental Protection Agency Mandatory Reporting of Greenhouse**

Gases. Available in: <http://www.epa.gov/>. Accessed in: 20 Sep. 2020.

EPBR. **Gás natural e o preço para a reindustrialização brasileira**. Available in: <https://epbr.com.br/gas-natural-e-o-preco-para-a-reindustrializacao-brasileira/>. Accessed in: 22 Oct. 2020.

EUROPEAN FERTILIZER MANUFACTURERS' ASSOCIATION. **Production of Ammonia**. In: Best Available Techniques for Pollution Prevention and Control in the European Fertilizer Industry. Brussels: Fisherprint Ltd, 2000. p. 42.

FLÓREZ-ORREGO, D.; DE OLIVEIRA JUNIOR, S. **On the efficiency, exergy costs and CO2 emission cost allocation for an integrated syngas and ammonia production plant**. Energy, v. 117, p. 341–360, 15 Dec. 2016.

FLÓREZ-ORREGO, D.; DE OLIVEIRA JUNIOR, S. **Modeling and optimization of an industrial ammonia synthesis unit: An exergy approach**. Energy, v. 137, p. 234–250, Oct. 2017.

FRATTINI, D.; CINTI, G.; BIDINI, G.; DESIDERI, U.; CIOFFI, R.; JANNELLI, E. **A system approach in energy evaluation of different renewable energies sources integration in ammonia production plants**. Renewable Energy, v. 99, p. 472–482, Dec. 2016.

GALE, J.; BRADSHAW, J.; CHEN, Z.; GARG, A.; GOMEZ, D.; ROGNER, H.-H.; SIMBECK, D.; WILLIAMS, R.; TOTH, F.; VAN VUUREN, D. **Sources of CO2**. In: EL GIZOULI, I.; HAKE, J. F. (Eds.). . Carbon dioxide capture and storage. 1st. ed. Cambridge University Press, 2005. p. 75–103.

GUNARDSON, H. H. **Industrial Gases in Petrochemical Processing**. Marcel Dekker, 1997.

GUOXUE, L.; JULIANG, C.; BENBIN, L.; DONGQING, G.; SHIQING, L.; GUOJUN, H.; XIN, D.; XULIANG, L.; HONGJUN, D.; HONGZHUAN, W.; WENBIN, Y.; XIANMING, G. **PSA hydrogen production process.** China, 27 Feb. 2013.

HALMANN, M. M.; MEYER, S. **Greenhouse Gas Carbon Dioxide Mitigation: Science and Technology**. Lewis Publishers, 1998.

HUMPHREYS, P. **Weigh the benefits of on-site nitrogen generation**. Available in: <https://www.plantengineering.com/articles/weigh-the-benefits-of-on-site-nitrogen-generation/>. Accessed in: 23 Nov. 2020.

IHS MARKIT. **Urea Fertilizer Market Outlook & Price Data | IHS Markit**. Available in: <https://agribusiness.ihsmarkit.com/sectors/fertilizers/urea.html>. Accessed in: 20 Sep. 2020a.

IHS MARKIT. **Ammonia | IHS Markit**. Available in: <https://agribusiness.ihsmarkit.com/sectors/fertilizers/ammonia.html>. Accessed in: 20 Sep. 2020b.

INSTITUTE FOR SUSTAINABLE PROCESS TECHNOLOGY. **Power to Ammonia**. Amersfoort: [s.n.]. Available in: <http://www.ispt.eu/media/ISPT-P2A-Final-Report.pdf>. Accessed in: 11 Apr. 2018.

INTERNATIONAL ENERGY ASSOCIATION. **Producing ammonia and fertilizers: new opportunities from renewables.** Available in: <https://www.iea.org/media/news/2017/Fertilizer_manufacturing_Renewables_01102017.pdf>. Accessed in: 28 Mar. 2018.

JUN, H. J.; PARK, M. J.; BAEK, S. C.; BAE, J. W.; HA, K. S.; JUN, K. W. **Kinetics modeling for the mixed reforming of methane over Ni-CeO 2/MgAl2O4 catalyst**. Journal of Natural Gas Chemistry, v. 20, n. 1, p. 9–17, 1 Jan. 2011.

KHADEMI, M. H.; SABBAGHI, R. S. **Comparison between three types of ammonia synthesis reactor configurations in terms of cooling methods**. Chemical Engineering Research and Design, v. 128, p. 306–317, 1 Dec. 2017.

KIM, A. R.; LEE, H. Y.; LEE, D. H.; KIM, B. W.; CHUNG, C. H.; MOON, D. J.; JANG, E. J.; PANG, C.; BAE, J. W. **Combined Steam and CO2 reforming of CH4 on LaSrNiOx mixed oxides supported on Al2O3-modified SiC support**. Energy and Fuels, v. 29, n. 2, p. 1055–1065, 2015.

KUMAR, N.; ROY, A.; WANG, Z.; L'ABBATE, E. M.; HAYNES, D.; SHEKHAWAT, D.; SPIVEY, J. J. **Bi-reforming of methane on Ni-based pyrochlore catalyst**. Applied Catalysis A: General, v. 517, p. 211–216, May 2016.

KUMAR, N.; SHOJAEE, M.; SPIVEY, J. J. **Catalytic bi-reforming of methane: From greenhouse gases to syngas**Current Opinion in Chemical Engineering, Aug. 2015. Available in: <https://linkinghub.elsevier.com/retrieve/pii/S2211339815000428>. Accessed in: 20 Jul. 2019

KYRIAKOU, V.; GARAGOUNIS, I.; VASILEIOU, E.; VOURROS, A.; STOUKIDES, M. **Progress in the Electrochemical Synthesis of Ammonia**. Catalysis Today, v. 286, p. 2–13, 15 May 2017.

LI, H.; SHANG, J.; SHI, J.; ZHAO, K.; ZHANG, L. **Facet-dependent solar ammonia synthesis of BiOCl nanosheets via a proton-assisted electron transfer pathway**. Nanoscale, v. 8, n. 4, p. 1986–1993, 2016.

LI, L.; ZHANG, L.; ZHANG, Y.; LI, J. **Effect of Ni loadings on the catalytic**

properties of Ni/MgO(111) catalyst for the reforming of methane with carbon dioxide. Journal of Fuel Chemistry and Technology, v. 43, n. 3, p. 315–322, Mar. 2015a.

LI, W.; ZHAO, Z.; REN, P.; WANG, G. **Effect of molybdenum carbide concentration on the Ni/ZrO2 catalysts for steam-CO2 bi-reforming of methane**. RSC Advances, v. 5, n. 122, p. 100865–100872, 23 Nov. 2015b.

LIU, H. **Ammonia synthesis catalyst 100 years: Practice, enlightenment and challenge**Cuihua Xuebao/Chinese Journal of CatalysisElsevier, , 1 Oct. 2014. Available in: <https://www.sciencedirect.com/science/article/pii/S1872206714601182>. Accessed in: 16 May. 2019

MACHADO, C. F. R.; ARAÚJO, O. DE Q. F.; DE MEDEIROS, J. L.; ALVES, R. M. DE B. **Carbon dioxide and ethanol from sugarcane biorefinery as renewable feedstocks to environment-oriented integrated chemical plants**. Journal of Cleaner Production, v. 172, p. 1232–1242, 20 Jan. 2018.

MAXWELL, G. R. **Synthetic Nitrogen Products - A practical guide to the products and processes**. Springer, 2005. v. 53

MEESSEN, J. **Urea synthesis**. Chemie-Ingenieur-Technik, v. 86, n. 12, p. 2180–2189, 2014.

MEESSEN, J. H. **Urea**. In: Ullmann's Encyclopedia of Industrial Chemistry. v. 37p. 657–695.

MIKURIYA, T.; YAGI, F.; SHIMURA, M. **Development of a new synthesis gas production catalyst and process with CO2 and H2O reforming**. AIChE 100 - 2008 AIChE Annual Meeting, Conference Proceedings. **Anais**... 2008. Available in: <https://folk.ntnu.no/skoge/prost/proceedings/aiche-2008/data/papers/P140551.pdf>. Accessed in: 21 Jul. 2019

MISSEN, R. W.; SMITH, W. R. **Chemical Reaction Stoichiometry (CRS): A Tutorial**. 1998.

MURZIN, D. Y. **Chemical reaction technology**. 1. ed. Turku: De Gruyter, 2015.

NIELSEN, A.; KJAER, J.; HANSEN, B. **Rate equation and mechanism of ammonia synthesis at industrial conditions**. Journal of Catalysis, v. 3, n. 1, p. 68–79, 1964.

OEC. **Urea - Product Trade, Exporters and Importers**. Available in: <https://oec.world/en/profile/hs92/urea-including-aqueous-solution-in-packs-10-kg>. Accessed in: 22 Oct. 2020.

OLAH, G. A.; GOEPPERT, A.; CZAUN, M.; PRAKASH, G. K. S. **Bi-reforming of methane from any source with steam and carbon dioxide exclusively to metgas (CO-**

2H2) for methanol and hydrocarbon synthesis. Journal of the American Chemical Society, v. 135, n. 2, p. 648–650, 2013.

OTTO, A.; GRUBE, T.; SCHIEBAHN, S.; STOLTEN, D. **Closing the loop: Captured CO2 as a feedstock in the chemical industry**. Energy and Environmental Science, v. 8, n. 11, p. 3283–3297, 2015.

ÖZKARA-AYDINOĞLU, Ş. **Thermodynamic equilibrium analysis of combined carbon dioxide reforming with steam reforming of methane to synthesis gas**. International Journal of Hydrogen Energy, v. 35, n. 23, p. 12821–12828, Dec. 2010.

PAL, D. B.; CHAND, R.; UPADHYAY, S. N.; MISHRA, P. K. **Performance of water gas shift reaction catalysts: A review**. Renewable and Sustainable Energy Reviews, v. 93, p. 549–565, 2018.

PENG, D. Y.; ROBINSON, D. B. **A New Two-Constant Equation of State**. Industrial and Engineering Chemistry Fundamentals, v. 15, n. 1, p. 59–64, Feb. 1976.

QIN, D.; LAPSZEWICZ, J.; JIANG, X. **Comparison of partial oxidation and steam-CO2 mixed reforming of CH4 to syngas on MgO-supported metals**. Journal of Catalysis, v. 159, n. 1, p. 140–149, Mar. 1996.

QUON, W. L. **A Compact and Efficient Steam Methane Reformer for Hydrogen Production**. University of Houston, 2012.

RAFIEE, A.; RAJAB KHALILPOUR, K.; MILANI, D.; PANAHI, M. **Trends in CO2 conversion and utilization: A review from process systems perspective**Journal of Environmental Chemical Engineering, Oct. 2018. Available in: <https://linkinghub.elsevier.com/retrieve/pii/S2213343718305189>. Accessed in: 15 Jul. 2019

RAHIMPOUR, M. R.; ARAB ABOOSADI, Z.; JAHANMIRI, A. H. **Synthesis gas production in a novel hydrogen and oxygen perm-selective membranes tri-reformer for methanol production**. Journal of Natural Gas Science and Engineering, v. 9, p. 149–159, 1 Nov. 2012.

RAJESH, J. K.; GUPTA, S. K.; RANGAIAH, G. P.; RAY, A. K. **Multiobjective optimization of steam reformer performance using genetic algorithm**. Industrial and Engineering Chemistry Research, v. 39, n. 3, p. 706–717, 2000.

RAJESH, J. K.; GUPTA, S. K.; RANGAIAH, G. P.; RAY, A. K. **Multi-objective optimization of industrial hydrogen plants**. Chemical Engineering Science, v. 56, n. 3, p. 999–1010, 1 Feb. 2001.

RASE, H. F. **Chemical reactor design for process plants, vol. 2**. New York:

Wiley, 1977.

RATNASAMY, C.; WAGNER, J. **Water gas shift catalysis.** Catalysis Reviews - Science and EngineeringTaylor & Francis, , Sep. 2009. Available in: <http://www.tandfonline.com/doi/abs/10.1080/01614940903048661>. Accessed in: 19 Jul. 2019

ROSTRUP-NIELSEN, J. R. **New aspects of syngas production and use**. Catalysis Today, v. 63, n. 2–4, p. 159–164, Dec. 2000.

SANDVIK. **SAFUREX.** Available in: <https://www.materials.sandvik/en/materials-center/material-datasheets/tube-and-pipe-seamless/safurex/?show=pdf>.

SCHIAROLI, N.; LUCARELLI, C.; SANGHEZ DE LUNA, G.; FORNASARI, G.; VACCARI, A. **Ni-based catalysts to produce synthesis gas by combined reforming of clean biogas**. Applied Catalysis A: General, v. 582, p. 117087, Jul. 2019.

SCHLÖGL, R. **Catalytic synthesis of ammonia - A "never-ending story"?**Angewandte Chemie - International EditionJohn Wiley & Sons, Ltd, , 9 May 2003. Available in: <http://doi.wiley.com/10.1002/anie.200301553>. Accessed in: 21 May. 2019

SHAH, Y. T. **Chemical energy from natural and synthetic gas**.

SINDIPETRO BA. **Petrobrás arrenda fábricas de fertilizantes por menos de 1% da expectativa de receita**. Available in: <http://www.sindipetroba.org.br/2019/petrobras-arrenda-fabricas-de-fertilizantes-por-menos-de-1-da-expectativa-de-receita/>. Accessed in: 22 Oct. 2020.

SINGH, S.; BAHARI, M. B.; ABDULLAH, B.; PHUONG, P. T. T.; TRUONG, Q. D.; VO, D. V. N.; ADESINA, A. A. **Bi-reforming of methane on Ni/SBA-15 catalyst for syngas production: Influence of feed composition**. International Journal of Hydrogen Energy, v. 43, n. 36, p. 17230–17243, Sep. 2018.

SIRCAR, S.; GOLDEN, T. C. **Purification of hydrogen by pressure swing adsorption**. Separation Science and Technology, v. 35, n. 5, p. 667–687, 5 Jan. 2000.

SOLIMAN, M. A.; EL-NASHAIE, S. S. E. H.; AL-UBAID, A. S.; ADRIS, A. **Simulation of steam reformers for methane**. Chemical Engineering Science, v. 43, n. 8, p. 1801–1806, 1988.

SONG, X.; GUO, Z. **Technologies for direct production of flexible H2/CO synthesis gas**. Energy Conversion and Management, v. 47, n. 5, p. 560–569, Mar. 2006.

SPEIGHT, J. G. **Chemical and process design handbook**. McGraw-Hill, 2002.

STAMICARBON B.V. **Avancore Technology**. Available in:

<https://www.youtube.com/watch?v=CsxIQ27JATU>. Accessed in: 9 May. 2018.

STAMICARBON B.V. **STAMICARBON, 70 YEARS OF KNOWLEDGE AND INNOVATION**Available in: <https://www.ureaknowhow.com/ukh2/images/stories/sponsors/stac/stamicarbon_70_years.pdf>. Accessed in: 8 May. 2018.

STROUD, T.; SMITH, T. J.; LE SACHÉ, E.; SANTOS, J. L.; CENTENO, M. A.; ARELLANO-GARCIA, H.; ODRIOZOLA, J. A.; REINA, T. R. **Chemical CO2 recycling via dry and bi reforming of methane using Ni-Sn/Al2O3 and Ni-Sn/CeO2-Al2O3 catalysts**. Applied Catalysis B: Environmental, v. 224, p. 125–135, May 2018.

SUTANTO, S.; DIJKSTRA, J. W.; PIETERSE, J. A. Z.; BOON, J.; HAUWERT, P.; BRILMAN, D. W. F. **CO2 removal from biogas with supported amine sorbents: First technical evaluation based on experimental data**. Separation and Purification Technology, v. 184, p. 12–25, 31 Aug. 2017.

TAHIR, B.; TAHIR, M.; AMIN, N. A. S. **Silver loaded protonated graphitic carbon nitride (Ag/pg-C3N4) nanosheets for stimulating CO2 reduction to fuels via photocatalytic bi-reforming of methane**. Applied Surface Science, v. 493, p. 18–31, 2019.

TAVARES, F. V; MONTEIRO, L. P. C.; MAINIER, F. B. **Indicators of energy efficiency in ammonia productions plants**. American Journal of Engineering Research, v. 02, n. 07, p. 116–123, 2013.

TEUNER, S. C.; NEUMANN, P.; VON LINDE, F. **The Calcor standard and Calcor economy processes**. Oil Gas European Magazine, v. 27, p. 44–46, 2001.

TONKOVICH, A. L. Y.; YANG, B.; PERRY, S. T.; FITZGERALD, S. P.; WANG, Y. **From seconds to milliseconds to microseconds through tailored microchannel reactor design of a steam methane reformer**. Catalysis Today, v. 120, n. 1, p. 21–29, Jan. 2007.

TRIMM, D. L. **Coke formation and minimisation during steam reforming reactions**. Catalysis Today, v. 37, n. 3, p. 233–238, Aug. 1997.

TURTON, R.; BAILIE, R. C.; WHITING, W. B.; SHAEIWIT, J. A. **Analysis, synthesis and design of chemical processes**. Pearson Education, 2008.

TURTON, R.; SHAEIWITZ, J. A.; BHATTACHARYYA, D.; WHITING, W. B. **Analysis, Synthesis, and Design of Chemical Processes**. 5th. ed. Prentice Hall, 2018.

ULRICH, G. D.; VASUDEVAN, P. T. **How to Estimate Utility Costs**. Chemical Engineering, p. 66–69, Apr. 2006.

UNION OF CONCERNED SCIENTISTS. **Uses of Natural Gas**. Available in:

<https://www.ucsusa.org/resources/uses-natural-gas>. Accessed in: 22 Oct. 2020.

UNITED STATES DEPARTMENT OF ENERGY. **Clean Coal Research Program**

UNITED STATES GEOLOGICAL SURVEY. **Nitrogen (Fixed) - Ammonia**. United States: 2018. Available in: <https://minerals.usgs.gov/minerals/pubs/commodity/nitrogen/mcs-2018-nitro.pdf>. Accessed in: 11 Apr. 2018.

VAN BEURDEN, P. **ON THE CATALYTIC ASPECTS OF STEAM-METHANE REFORMING A Literature Survey**. ECN, n. December, 2004.

VERNON, P. D. F.; GREEN, M. L. H.; CHEETHAM, A. K.; ASHCROFT, A. T. **Partial oxidation of methane to synthesis gas, and carbon dioxide as an oxidising agent for methane conversion**. Catalysis Today, v. 13, n. 2–3, p. 417–426, 27 Mar. 1992.

VON DER ASSEN, N.; JUNG, J.; BARDOW, A. **Life-cycle assessment of carbon dioxide capture and utilization: avoiding the pitfalls**. Energy & Environmental Science, v. 6, n. 9, p. 2721–2734, Aug. 2013.

VOZNIUK, O.; TANCHOUX, N.; MILLET, J. M.; ALBONETTI, S.; DI RENZO, F.; CAVANI, F. **Spinel Mixed Oxides for Chemical-Loop Reforming: From Solid State to Potential Application**. In: Studies in Surface Science and Catalysis. Elsevier, 2019. v. 178p. 281–302.

WAES, J. P. M. VAN. **Preparation of Urea**United States, 1950. Available in: <https://patents.google.com/patent/US2727069>. Accessed in: 7 Mar. 2018

WILHELM, D. J.; SIMBECK, D. R.; KARP, A. D.; DICKENSON, R. L. **Syngas production for gas-to-liquids applications: Technologies, issues and outlook**. Fuel Processing Technology, v. 71, n. 1–3, p. 139–148, Jun. 2001.

XU, J.; FROMENT, G. F. **Methane steam reforming, methanation and water-gas shift: I. Intrinsic kinetics**. AIChE Journal, v. 35, n. 1, p. 88–96, 1989a.

XU, J.; FROMENT, G. F. **Methane steam reforming: II. Diffusional limitations and reactor simulation**. AIChE Journal, v. 35, n. 1, p. 97–103, Jan. 1989b.

YORK, A. P. E.; SUHARTANTO, T.; GREEN, M. L. H. **Influence of molybdenum and tungsten dopants on nickel catalysts for the dry reforming of methane with carbon dioxide to synthesis gas**. Studies in Surface Science and Catalysis, v. 119, p. 777–782, 1998.

YUAN, M. **Managing Energy in Fertilizer Production and Use**. Available in: <http://large.stanford.edu/courses/2014/ph240/yuan2/>. Accessed in: 29 Jul. 2019.

APPENDIX A

The following tables show utilities usage, costs, and CO_2 emission rates for the conventional and innovative routes, respectively.

Table A1 – Breakdown of utilities usage and CO_2 emissions for the equipment in the conventional route.

Equipment	Utility	Duty (GJ/h)	Usage (tonne/h)*	Cost (MM$/year)	CO_2 emission rate (tonne/h)
C-X11	ELEC	11.81	3.28*	2.23	1.14
C-X12	ELEC	37.65	10.46*	7.11	3.63
C-X41	ELEC	57.89	16.08*	10.93	5.58
C-X61	ELEC	35.09	9.75*	6.62	3.38
E-X11		295.25			
E-X21	MPSg	78.44	38.55	-1.51	-5.16
E-X22	CW	157.71	7546.29	0.29	
E-X31		56.75			
E-X32	CW	162.44	7772.57	0.30	
E-X33	MPS	311.57	153.12	6.01	20.49
E-X34	CW	148.73	7116.51	0.28	
E-X41	CW	58.07	2778.84	0.11	
E-X51		98.31			
E-X52	CW	232.21	11111.20	0.43	
E-X61	LPS	2.27	1.04	0.04	0.15
E-X62	HPSg	22.06	12.83	-0.48	-1.45
H-X31	FH	45.80	0.92	1.63	2.51
P-X11	ELEC	0.29	0.08*	0.06	0.03
P-X31	ELEC	2.03	0.57*	0.38	0.20
R-X11	FH	311.63	6.23	11.08	17.09
Total:				45.50	47.58

(*): Values of "Usage" for the ELEC utility are expressed in MW.

Table A2 – Breakdown of utilities usage and CO_2 emissions for the equipment in the innovative route

Equipment	Utility	Duty (GJ/h)	Usage (tonne/h)*	Cost (MM$/year)	CO_2 emission rate (tonne/h)
C-Y11	ELEC	21.05	5.84*	3.97	2.03
C-Y31	ELEC	93.06	25.85*	17.56	8.97
C-Y51	ELEC	33.58	9.33*	6.34	3.24
E-Y11	LPS	2.33	1.06	0.04	0.15
E-Y12		124.40			
E-Y13	CW	163.39	7818.21	0.30	
E-Y21		24.13			
E-Y22	CW	33.39	1597.77	0.06	
E-Y23	MPS	85.86	42.20	1.66	5.65
E-Y24	CW	40.82	1953.04	0.08	
E-Y25	CW	13.25	633.94	0.02	
E-Y41		75.13			
E-Y42	CW	251.16	12017.80	0.47	
E-Y51	CW	6.05	289.37	0.01	
E-Y52	HPSg	20.68	12.03	-0.45	-1.36
E-Y53	LPS	2.24	1.02	0.04	0.15
P-Y11	ELEC	0.02	0.00*	0.00	0.00
P-Y21	ELEC	0.22	0.06*	0.04	0.02
R-Y11	FH	500.53	10.00	17.79	27.45
PSA	ELEC	1.29	0.36	0.24	0.12
Total:				48.18	46.42

(*): Values of "Usage" for the ELEC utility are expressed in MW.

APPENDIX B

The following tables show equipment costs for the conventional and innovative routes, respectively.

Table B1 – Equipment costs for the conventional route.

Equipment	Purchased Equipment Cost ($)	Bare Module Cost ($)	Total Module Cost ($)	Grass Roots Cost ($)
C-X11	1,250,000	3,410,000	4,190,000	5,970,000
C-X12	3,420,000	19,700,000	23,200,000	27,900,000
C-X61	821,000	4,720,000	5,570,000	6,690,000
C-X41	5,220,000	14,300,000	17,600,000	25,000,000
D-X11	333,000	499,000	589,000	838,000
D-X12	875,000	1,310,000	1,550,000	2,200,000
D-X61	721,000	1,080,000	1,280,000	1,820,000
D-X41	1,250,000	1,870,000	2,210,000	3,140,000
E-X11	47,000	223,000	263,000	340,000
E-X21	54,200	257,000	304,000	393,000
E-X22	103,000	344,000	406,000	574,000
E-X31	96,400	317,000	374,279	533,000
E-X34	172,000	567,000	700,000	950,000
E-X32	202,000	664,000	783,000	1,120,000
E-X41	47,300	158,000	200,000	265,000
E-X52	796,000	4,100,000	4,830,000	6,140,000
E-X61	5,820	22,800	28,100	38,000
E-X51	123,000	976,000	1,152,000	1,360,000
E-X33	2,790,000	9,200,000	10,860,000	15,400,000
E-X62	28,100	160,000	188,704	235,000
R-X11	9,800,000	26,000,000	32,000,000	42,800,000
R-X12	513,000	1,340,000	1,650,000	2,220,000
H-X31	1,510,000	3,270,000	3,860,000	5,460,000
P-X11	17,600	89,400	105,000	134,000
P-X31	86,300	439,000	518,000	660,000
T-X31	146,000	1,200,000	1,420,000	1,580,000
T-X32	695,000	1,470,000	1,730,000	2,290,000
R-X21	60,900	1,060,000	1,250,000	1,340,000
R-X22	65,000	1,130,000	1,330,000	1,430,000
R-X31	32,600	566,000	670,000	720,000
V-X21	27,100	345,000	408,000	463,000

V-X31	30,400	124,000	146,000	208,000
V-X41	16,200	172,000	203,000	236,000
V-X51	157,000	26,200,000	30,900,000	31,200,000
BED1	13,300	3,100,000	3,660,000	3,680,000
BED2	16,200	3,780,000	4,460,000	4,490,000
BED3	21,000	4,910,000	5,800,000	5,830,000
Total*	44,187,388	194,702,480	232,960,000	287,840,000

(*): Total prices include the nationalization factor of 1.4 for Brazil.

Table B2 – Equipment costs for the innovative route.

Equipment	Purchased Equipment Cost ($)	Bare Module Cost ($)	Total Module Cost ($)	Grass Roots Cost ($)
C-Y11	1,840,000	5,040,000	6,190,000	8,820,000
C-Y31	8,180,000	22,400,000	26,400,000	37,600,000
C-Y51	3,170,000	18,200,000	21,500,000	25,800,000
D-Y11	517,000	776,000	916,000	1,300,000
D-Y31	1,820,000	2,730,000	3,220,000	4,580,000
D-Y51	714,000	1,070,000	1,260,000	1,800,000
E-Y11	23,900	78,600	93,000	132,000
E-Y13	87,000	406,000	479,143	622,000
E-Y24	63,700	209,000	250,000	352,000
E-Y22	61,000	201,000	237,000	337,000
E-Y42	775,000	3,990,000	4,902,000	6,200,000
E-Y53	5,820	22,800	30,000	38,000
E-Y21	57,200	188,000	221,903	316,000
E-Y52	26,800	153,000	180,000	224,000
E-Y23	769,000	2,540,000	2,996,000	4,260,000
E-Y12	39,100	243,000	286,000	351,000
E-Y25	28,300	93,600	110,406	157,000
E-Y51	29,200	96,100	113,000	162,000
R-Y11	16,300,000	45,700,000	56,200,000	74,200,000
P-Y11	5,380	21,400	26,400	35,400
P-Y21	8,720	34,700	41,000	55,100
T-Y21	134,000	609,000	720,000	870,000
T-Y22	85,100	236,000	279,000	380,000
V-Y11	42,000	307,000	377,000	467,000
V-Y21	8,710	35,400	41,800	59,500
V-Y23	37,400	266,000	327,000	407,000
V-Y41	136,000	21,600,000	25,500,000	25,700,000
BED1	13,300	3,100,000	3,660,000	3,680,000
BED2	16,200	3,780,000	4,460,000	4,490,000
BED3	21,000	4,910,000	5,800,000	5,830,000
PSA	2,157,958	8,668,408	10,228,722	14,562,926
Total*	52,041,903	206,787,011	247,863,523	313,303,096

(*): Total prices include the nationalization factor of 1.4 for Brazil.

APPENDIX C

This Appendix briefly describes some of the relevant economic parameters used in the cash flow analysis (Subsection 7.8.2) and in the sensitivity analysis (Subsection 7.8.3).

Most of the relevant economic indicators were taken from the default values of the CAPCOST sheet and were equally applied to both routes. They are:

- A Chemical Engineering Plant Cost Index (CEPCI) of 619.2 (preliminary value of January 2019);
- Project life: 15 years;
- Construction period: 2 years;
- Distribution of fixed capital investment: 60% at the end of year one and 40% at the end of year two;
- Fixed capital investment: grassroots costs (Appendix B) were used, since both plants were constructed from scratch;
- Cost of land: $1,250,000;
- Taxation rate: 42%;
- Annual interest rate: 10%;
- Salvage value (considering complete plant shutdown after project life): 10% of the fixed capital investment;
- Cost of operating labor per operator: $72,570/year;
- Number of operators: 15 for the BRM process and 16 for the SRM process (based on the number of plant equipment);
- Depreciation method: Modified Accelerated Cost Recovery System (MACRS) over 10 years.